

Accelerated Article Preview

BA.2.12.1, BA.4 and BA.5 escape antibodies elicited by Omicron infection

Received: 30 April 2022

Accepted: 15 June 2022

Accelerated Article Preview

Cite this article as: Cao, Y. et al. BA.2.12.1, BA.4 and BA.5 escape antibodies elicited by Omicron infection. *Nature* <https://doi.org/10.1038/s41586-022-04980-y> (2022)

Yunlong Cao, Ayijiang Yisimayi, Fanchong Jian, Weiliang Song, Tianhe Xiao, Lei Wang, Shuo Du, Jing Wang, Qianqian Li, Xiaosu Chen, Yuanling Yu, Peng Wang, Zhiying Zhang, Pulan Liu, Ran An, Xiaohua Hao, Yao Wang, Jing Wang, Rui Feng, Haiyan Sun, Lijuan Zhao, Wen Zhang, Dong Zhao, Jiang Zheng, Lingling Yu, Can Li, Na Zhang, Rui Wang, Xiao Niu, Sijie Yang, Xuetao Song, Yangyang Chai, Ye Hu, Yansong Shi, Linlin Zheng, Zhiqiang Li, Qingqing Gu, Fei Shao, Weijin Huang, Ronghua Jin, Zhongyang Shen, Youchun Wang, Xiangxi Wang, Junyu Xiao & Xiaoliang Sunney Xie

This is a PDF file of a peer-reviewed paper that has been accepted for publication. Although unedited, the content has been subjected to preliminary formatting. Nature is providing this early version of the typeset paper as a service to our authors and readers. The text and figures will undergo copyediting and a proof review before the paper is published in its final form. Please note that during the production process errors may be discovered which could affect the content, and all legal disclaimers apply.

BA.2.12.1, BA.4 and BA.5 escape antibodies elicited by Omicron infection

Yunlong Cao^{1,2,#,*}, Ayijiang Yisimayi^{1,3,#}, Fanchong Jian^{1,4,#}, Weiliang Song^{1,3,#}, Tianhe Xiao^{1,5,#},
Lei Wang^{6,#}, Shuo Du^{3,#}, Jing Wang^{1,3,#}, Qianqian Li^{7,#}, Xiaosu Chen^{8,#}, Yuanling Yu^{2,7,#}, Peng
Wang², Zhiying Zhang³, Pulan Liu³, Ran An¹, Xiaohua Hao⁹, Yao Wang², Jing Wang², Rui Feng⁶,
Haiyan Sun², Lijuan Zhao², Wen Zhang⁹, Dong Zhao⁹, Jiang Zheng², Lingling Yu², Can Li², Na
Zhang², Rui Wang², Xiao Niu^{1,4}, Sijie Yang^{1,10}, Xuetao Song², Yangyang Chai⁸, Ye Hu⁸, Yansong
Shi⁸, Linlin Zheng², Zhiqiang Li^{10,11}, Qingqing Gu², Fei Shao², Weijin Huang⁷, Ronghua Jin⁹,
Zhongyang Shen^{12,*}, Youchun Wang^{2,7,*}, Xiangxi Wang^{2,6,*}, Junyu Xiao^{2,3,10,11,*}, Xiaoliang
Sunney Xie^{1,2,*}

¹Biomedical Pioneering Innovation Center (BIOPIC), Peking University, Beijing, P.R. China.

²Changping Laboratory, Beijing, P.R. China.

³School of Life Sciences, Peking University, Beijing, P.R. China.

⁴College of Chemistry and Molecular Engineering, Peking University, Beijing, P.R. China.

⁵Joint Graduate Program of Peking-Tsinghua-NIBS, Academy for Advanced Interdisciplinary Studies, Peking University, Beijing, China.

⁶CAS Key Laboratory of Infection and Immunity, National Laboratory of Macromolecules, Institute of Biophysics, Chinese Academy of Sciences, Beijing, P.R. China.

⁷Division of HIV/AIDS and Sex-transmitted Virus Vaccines, Institute for Biological Product Control, National Institutes for Food and Drug Control (NIFDC), Beijing, P.R. China.

⁸Institute for Immunology, College of Life Sciences, Nankai University, Tianjin, P. R. China.

⁹Beijing Ditan Hospital, Capital Medical University, Beijing, P.R. China.

¹⁰Peking-Tsinghua Center for Life Sciences, Peking University, Beijing, P.R. China

¹¹Academy for Advanced Interdisciplinary Studies, Peking University, Beijing, P.R. China.

¹²Organ Transplant Center, NHC Key Laboratory for Critical Care Medicine, Tianjin First Central Hospital, Nankai University, Tianjin, P. R. China.

*Correspondence: Yunlong Cao (yunlongcao@pku.edu.cn); Zhongyang Shen (zhongyangshen@nankai.edu.cn); Youchun Wang (wangyc@nifdc.org.cn); Xiangxi Wang (xiangxi@ibp.ac.cn); Junyu Xiao (junyuxiao@pku.edu.cn); Xiaoliang Sunney Xie (sunneyxie@biopic.pku.edu.cn)

30 #These authors contributed equally.

31

32 **Abstract**

33 SARS-CoV-2 Omicron sublineages BA.2.12.1, BA.4 and BA.5 exhibit higher transmissibility
34 over BA.2¹. The new variants' receptor binding and immune evasion capability require immediate
35 investigation. Here, coupled with Spike structural comparisons, we show that BA.2.12.1 and
36 BA.4/BA.5 exhibit comparable ACE2-binding affinities to BA.2. Importantly, BA.2.12.1 and
37 BA.4/BA.5 display stronger neutralization evasion than BA.2 against the plasma from 3-dose
38 vaccination and, most strikingly, from post-vaccination BA.1 infections. To delineate the
39 underlying antibody evasion mechanism, we determined the escaping mutation profiles², epitope
40 distribution³ and Omicron neutralization efficacy of 1640 RBD-directed neutralizing antibodies
41 (NAbs), including 614 isolated from BA.1 convalescents. Interestingly, post-vaccination BA.1
42 infection mainly recalls wildtype-induced humoral memory. The resulting elicited antibodies
43 could neutralize both wildtype and BA.1 and are enriched on non-ACE2-competing epitopes.
44 However, most of these cross-reactive NAbs are heavily escaped by L452Q, L452R and F486V.
45 BA.1 infection can also induce new clones of BA.1-specific antibodies that potently neutralize
46 BA.1; nevertheless, these NAbs are largely escaped by BA.2/BA.4/BA.5 due to D405N and
47 F486V, and react weakly to pre-Omicron variants, exhibiting poor neutralization breadths. As for
48 therapeutic NAbs, Bectelovimab⁴ and Cilgavimab⁵ can effectively neutralize BA.2.12.1 and
49 BA.4/BA.5, while the S371F, D405N and R408S mutations would undermine most broad
50 sarbecovirus NAbs. Together, our results indicate that Omicron may evolve mutations to evade
51 the humoral immunity elicited by BA.1 infection, suggesting that BA.1-derived vaccine boosters
52 may not achieve broad-spectrum protection against new Omicron variants.

53

54

55

56

57

58

59 **Main**

60 The recent emergence and global spreading of severe acute respiratory syndrome coronavirus 2
61 (SARS-CoV-2) variant Omicron (B.1.1.529) have posed a critical challenge to the efficacy of
62 COVID-19 vaccines and neutralizing antibody therapeutic⁶⁻⁹. Due to multiple mutations to the
63 spike protein, including its receptor-binding domain (RBD) and N-terminal domain (NTD),
64 Omicron BA.1 can cause severe neutralizing antibody evasion^{3,10-13}. Currently, Omicron
65 sublineage BA.2 has rapidly surged worldwide, out-competing BA.1. Compared to the RBD of
66 BA.1, BA.2 contains three additional mutations, including T376A, D405N and R408S, and lacks
67 the G446S and G496S harbored by BA.1 ([Extended Data Fig. 1a](#)). The S371L on BA.1 is also
68 substituted with S371F in BA.2. Importantly, new Omicron variants are still continuously
69 emerging. The recently appeared new Omicron variants contain identical RBD sequences to BA.2
70 but with the addition of L452 and F486 substitutions, namely BA.2.12.1 (L452Q), BA.2.13
71 (L452M), BA.4 and BA.5 (L452R+F486V), and all displayed higher transmission advantage over
72 BA.2. The new variants' receptor binding and immune evasion capability require immediate
73 investigation.

74 **Structural analyses of Omicron Spike**

75 First, we expressed and purified the prefusion-stabilized trimeric ectodomains of BA.1, BA.2,
76 BA.3, BA.2.12.1, BA.2.13 and BA.4/BA.5 Spike (S-trimer). Noteworthy, BA.4 and BA.5 share
77 the same spike mutations. All spike-trimers contain GSAS and 6P mutations along with the T4
78 fibrin trimerization domain for stabilization purpose^{14,15}. We determined the cryo-EM
79 reconstructions of these S-trimers at an overall resolution of 3.1-3.5 Å, together with our previous
80 reported BA.1 structure, allowing us to compare the detailed structural variations across Omicron
81 sublineages ([Fig. 1a](#) and [Extended Data Fig. 1b](#)). Distinct from stably maintaining an open
82 conformation with one 'up' RBD and two 'down' RBDs observed in BA.1 S-trimer¹⁶, BA.2 and
83 BA.2.12.1 exhibit two conformational states corresponding to a closed-form with all three RBDs
84 "down" and an open form with one RBD "up". Notably, one RBD was clearly disordered,
85 representing a stochastic movement in BA.2.13, which, together with BA.2 and BA.2.12.1,

86 suggests structural heterogeneity in the S-trimers of BA.2 sublineages. Surprisingly, most BA.3
87 and BA.4 S-trimers adopt closed- or semi-closed forms (Fig. 1a). The RBD confirmation
88 differences could be allosterically modulated by mutations/deletions in NTD or near the furin
89 cleavage site, with the detailed mechanism unclear. Also, the BA.4/5 spike we used contains the
90 N658S mutation, which was presented in early BA.4/5 sequences but later disappeared due to a
91 disadvantage in transmissibility, and may correlate with BA.4/5's more closed RBD configurations.
92 Interestingly, BA.2 sublineage S-trimers harbor relatively less compacted architectures in the
93 region formed by the three copies of S2 (Fig. 1b). By contrast, BA.1, BA.3 and BA.4/BA.5 possess
94 relatively tight inter-subunit organization with the more buried areas between S2 subunits (Fig.
95 1b). In line with structural observations, thermal stability assays also verified that S-trimers from
96 BA.2 sublineages were the least stable among these variants, which might confer enhanced fusion
97 efficiencies (Fig. 1c).

98
99 Next, we measured the binding affinity between hACE2 and S-trimers of the Omicron variants by
100 surface plasmon resonance (SPR) (Extended Data Fig. 1c). BA.4/5 spike trimer showed a
101 decreased hACE2 binding affinity than other Omicron subvariants; however, this measurement
102 could be deficient due to the additional N658S mutation. To exclude N658S's potential influence,
103 the binding affinities between hACE2 and Omicron variants' RBDs are also examined (Fig. 1d).
104 The RBD of Delta and all circulating Omicron subvariants exhibited similar ACE2 binding affinity,
105 except for BA.3, which showed lower affinity, comparable to that of the wildtype (WT) strain.
106 Additionally, the BA.2 subvariants displayed slightly increased hACE2 binding affinities than
107 other Omicron variants. To further explore the molecular basis for altered binding affinities of
108 these variants to hACE2, we performed molecular dynamics (MD) simulations based on cryo-EM
109 structures and examined the effect of the RBD residue substitutions on the interaction with hACE2
110 (Extended Data Fig. 1d). Results revealed that the lack of G496S in BA.2 sublineages retained the
111 hydrogen bond with K353 to hACE2, increasing their binding capability, which is in line with
112 experimental observations revealed by deep mutational scanning assay¹⁷. Unexpectedly, a local
113 conformational perturbation surrounding residues 444-448 lost its hydrophilic interaction

114 between S446 with Q42 from hACE2 in BA.3, which is presumably caused by the single mutation
115 G446S rather than double mutations of G446S and G496S (Extended Data Fig. 1d). Remarkably,
116 F486V carried by BA.4/5 decreases hACE2 binding activity due to reduced hydrophobic
117 interaction (Extended Data Fig. 1d). Potential hydrophilic interaction reduction could also be
118 observed due to R493Q reversion. Notably, two recent reports claimed that BA.4/5 RBD and Spike
119 (S2P) showed higher binding affinity to hACE2 compared to BA.1 and BA.2, due to L452R and
120 R493Q reversion^{18,19}. Despite the discrepancy, it can be concluded that BA.2 subvariants and
121 BA.4/5 were able to maintain high hACE2 binding affinity.

122 **NAb evasion of BA.2.12.1, BA.4 and BA.5**

123 To probe the neutralization evasion ability of the recently emerged Omicron sublineages, we
124 performed pseudovirus neutralization assays using D614G, BA.1, BA.1.1, BA.2, BA.3, BA.2.12.1,
125 BA.2.13 and BA.4/BA.5 against the plasma obtained from 3-dose vaccinated individuals, BA.1
126 convalescents with previous vaccination, and vaccinated SARS convalescents (Supplementary
127 Table 1). Plasma samples were collected 4 weeks after the booster shot or 4 weeks after COVID-
128 19 hospital discharge. In individuals that received CoronaVac or ZF2001 booster six months after
129 two doses of inactivated vaccine (CoronaVac), BA.1, BA.1.1 and BA.2 showed no significant
130 difference in plasma neutralization resistance (Fig. 2a-b), concordant with previous reports^{20,21}.
131 However, we found that BA.2 subvariants BA.2.13 and BA.2.12.1 showed increased immune
132 evasion capability than BA.2, with BA.2.12.1 stronger than BA.2.13, and BA.4/BA.5 conferring
133 even stronger antibody escape (Fig. 2a-b). The drop of neutralization titers is more obvious in the
134 plasma obtained from individuals infected by BA.1 who had received 3-dose CoronaVac before
135 infection (Fig. 2c), despite their significantly higher neutralization against D614G and BA.1
136 compared to the 3-dose vaccinees without BA.1 infection (Extended Data Fig. 2a). The plasma
137 NT50 of BA.1 convalescents against BA.2.13, BA.2.12.1 and BA.4/5, compared to that against
138 BA.1, was reduced by 2.0x, 3.7x and 8.0x fold, respectively. Interestingly, plasma from vaccinated
139 SARS convalescents showed a different phenotype than normal vaccinees, such that BA.2
140 subvariants and BA.3/BA.4/BA.5 could cause a striking neutralization loss (Fig. 2d and Extended

141 [Data Fig. 2b](#)). This suggests that certain mutations in BA.2 lineages and BA.3/4/5 may specifically
142 evade broad sarbecovirus neutralizing antibodies, which are substantially enriched in vaccinated
143 SARS convalescents²². Together, these observations indicate that the newly emerged BA.2.12.1
144 and BA.4/5 display stronger and distinct humoral immune evasion than BA.1.

145 Next, we examined the reaction difference in neutralizing activities of therapeutic antibodies
146 against new Omicron subvariants ([Fig. 2e](#)). All of the seven Omicron subvariants displayed
147 striking evasion against neutralization by Class 1 and 2 RBD antibodies, such that REGN-10933
148 (Casirivimab)²³, LY-CoV016 (Etesevimab)²⁴ and LY-CoV555 (Bamlanivimab)²⁵, COV2-2196
149 (Tixagevimab)⁵ and BR11-196 (Amubarvimab)²⁶ were strongly affected, while DXP-604^{15,27} were
150 evaded only by BA.4/5, showing reduced but still competitive efficacy against BA.1 and BA.2
151 subvariants. Two major antigenicity differences were observed between BA.1 and BA.2
152 subvariants. First, neutralizing antibodies targeting the linear epitope 440-449³, such as REGN-
153 10987 (Imdevimab)²³, COV2-2130 (Cilgavimab, component of Evusheld)⁵ and LY-CoV1404
154 (Bebtelovimab)⁴ can neutralize BA.2 subvariants and BA.4/5. Second, BA.2 sublineages greatly
155 reduce the efficacy of BA.1-effective broad sarbecovirus neutralizing antibodies, including ADG-
156 2 (Adintrevimab)²⁸ and S309 (Sotrovimab)²⁹, except the ACE2-mimicking antibody S2K146³⁰,
157 which potently neutralize all BA.1 and BA.2 sublineages but showed reduced activity against
158 BA.4/5, similar to DXP-604. BR11-196 and BR11-198 cocktail (Amubarvimab/Romlusevimab)
159 were escaped by BA.2 sublineages⁹ and BA.3/BA.4/BA.5. Notably, LY-CoV1404⁴ demonstrated
160 high potency against all assayed Omicron subvariants. In addition, our recently developed non-
161 competing antibody cocktail isolated from vaccinated SARS convalescents, namely SA58 (BD55-
162 5840, Class 3) and SA55 (BD55-5514, Class 1/4), displayed high potency against all Omicron
163 subvariants and sarbecoviruses SARS-CoV-1, Pangolin-GD and RaTG13.

164
165 To delineate the underlying antibody evasion mechanism of BA.2.13, BA.2.12.1 and BA.4/BA.5,
166 especially on how they escape the humoral immunity induced by BA.1 convalescents and
167 vaccinated SARS convalescents, we started by isolating RBD-targeting NAb from those

168 individuals (Extended Data Fig. 3a)^{27,31}. First, antigen-specific memory B cells were isolated by
169 fluorescence-activated cell sorting (FACS) from pooled PBMCs using double RBD^{WT}+ selection
170 for 3-dose vaccinees, RBD^{WT}+ RBD^{SARS}+ selection for vaccinated SARS convalescents and
171 double RBD^{BA.1}+ selection for BA.1 convalescents (Extended Data Fig. 3b). Secondly, we
172 performed single-cell V(D)J sequencing (scVDJ-seq) with RBD^{BA.1} and RBD^{WT} feature barcodes
173 to the CD27⁺/IgM⁻ antigen-specific memory B cells (Extended Data Fig. 3b). Thirdly, we extracted
174 the productive heavy-light chain paired VDJ sequences and expressed the antibodies *in vitro* as
175 human IgG1. Interestingly, during this process, we found that the majority of Omicron-reactive
176 memory B cells from BA.1 convalescents who received 3-dose ComonaVac could also bind to
177 WT RBD (Fig. 3a). In contrast, only around one-fourth of Omicron-reactive memory B cells
178 isolated from unvaccinated BA.1 convalescents could bind to WT RBD (Fig. 3a). Also, the cross-
179 reactive antigen-binding property could only be observed in IgM-CD27⁺ memory B cells, but not
180 IgM+CD27⁻ naïve B cells (Extended Data Fig. 2b). VDJ sequence analysis revealed significantly
181 higher heavy chain V-domain somatic hypermutation (SHM) rates of BA.1/WT cross-reactive B
182 cell receptors (BCRs) than that of BA.1-specific BCRs (Fig. 3b), which implies that cross-reactive
183 memory B cells were further affinity-matured compared to BA.1-specific memory B cells.
184 Together, these suggest that post-vaccination infection with Omicron BA.1 mainly recalls WT-
185 induced memory B cells.

186 To further specify the epitope distribution of NAbs elicited by post-vaccination BA.1 infection,
187 we applied high-throughput yeast-display-based deep mutational scanning (DMS) assays^{2,3} and
188 successfully determined the escaping mutation profiles of 1640 RBD-binding antibodies. Among
189 these antibodies, 602 were from SARS-CoV-2 WT convalescents or 3-dose vaccinees, 614 from
190 post-vaccination BA.1 convalescents, and 410 SARS/WT cross-reactive antibodies from
191 vaccinated SARS convalescents (Supplementary Table 2). 14 antibodies with published DMS
192 profiles are also included^{2,32,33}. It is important to note that, among the 614 antibodies from post-
193 vaccination BA.1 convalescents, 102 are BA.1-specific and do not bind to WT RBD. The escaping
194 mutation profiles of those 102 BA.1-specific NAbs were determined by DMS based on BA.1 RBD.

195 The remaining 1538 RBD^{WT}-reactive antibodies were unsupervised clustered into 12 epitope
196 groups according to their WT-based mutational escaping profiles using t-distributed stochastic
197 neighbor embedding (t-SNE) (Fig. 3c), adding 6 more epitope groups compared to our previous
198 classification³.

199
200 Group A-C recapitulates our previous taxonomy³, in which the members mainly target the ACE2-
201 binding motif³⁴⁻³⁸ (Fig. 3h). Group D antibodies, such as REGN10987, LY-CoV1404 and COV2-
202 2130, bind to the linear epitope 440-449 on the RBD and are unsupervised expanded into D1 and
203 D2 subgroups. Group D1 is more affected by R346 and L452, while D2 antibodies do not and
204 interact more with P499 (Fig. 3h). Additionally, Group E and F are now expanded into E1-E3 and
205 F1-F3, which covers the front and backside of RBD, roughly corresponding to Class 3 and Class
206 4, respectively³⁷ (Fig. 3h). Group E1 corresponds to the S309 binding site, whose epitope involves
207 G339, T345 and R346. Group E2 antibodies bind to the front chest of RBD³⁵, where E2.1 is more
208 affected by R346 and A348, while E2.2 is more affected by K356 and R357. Group E3 (S2H97
209 site) and F1 (S304 site) bind to highly conserved regions on the bottom of RBD, mainly contacting
210 with K462/E516/L518, and S383/T385/K386, respectively. Group E1-E3 and F1 antibodies do not
211 compete with ACE2 (Fig. 3f), while F2 and F3 antibodies are ACE2-competing and affected by
212 T376, K378, D405, R408 and G504, corresponding to Class 1/4³⁹. Pseudovirus neutralizing
213 efficacy of antibodies in each group against SARS-CoV-1, SARS-CoV-2 D614G, Pangolin-GD
214 and RaTG13 is tested, and their binding capability to 22 sarbecovirus RBDs is measured through
215 ELISA (Supplementary Table 2 and Supplementary Table 3). We found that antibodies of the same
216 cluster have unified sarbecovirus neutralization potency and binding spectra (Fig. 3g and Extended
217 Data Fig. 4). In total, five clusters of antibodies exhibiting broad sarbecovirus binding ability were
218 identified, namely Groups E1, E3, F1, F2 and F3 (Extended Data Fig. 4), of which E1, F2 and F3
219 showed potent neutralizing activity against SARS-CoV-1 (Fig. 3g).

220
221 Importantly, we found that the individuals who experienced post-vaccination BA.1 infection
222 displayed enrichment of Group E2.1, E2.2 and F1 antibodies (Fig. 3d-e), which do not compete

223 with ACE2 (Fig. 3f). BA.1 does not harbor mutations on the epitopes of these NAb groups, which
224 may explain why post-vaccination BA.1 infection is more likely to stimulate those NAbs. Though
225 not enriched, the ACE2-competing Group B and D1 antibodies remain highly abundant. Since
226 Group E2, D1 and B antibodies are sensitive to 452 and 486 mutations (Fig. 3h), it is highly
227 possible that the newly emerged BA.2.12.1, BA.2.13, BA.4/BA.5 can specifically target those
228 antibodies, rationalizing the huge loss in NT50 of BA.1 convalescents' plasma against those
229 variants (Fig. 2c).

230 To examine our hypothesis, we measured pseudovirus neutralization of those NAbs against
231 BA.2.12.1, BA.2.13 and BA.4/BA.5, as well as the major Omicron variants BA.1, BA.1.1, BA.2
232 and BA.3 (Extended Data Fig. 5). Interestingly, NAbs from different epitope groups displayed
233 distinct neutralizing activities against Omicron subvariants. Also, BA.1-stimulated antibodies
234 (from BA.1 convalescents) and WT-stimulated (from WT convalescents or vaccinees, with or
235 without previous SARS-CoV-1 infection) showed significantly higher potency and breadth in most
236 epitope groups, confirming the higher affinity maturation (Extended Data Fig. 5).

237 Most WT-stimulated Group A, B and C NAbs were escaped by Omicron subvariants, while a
238 subset showed broad Omicron effectiveness (Extended Data Fig. 5). Those broad NAbs are largely
239 enriched by BA.1 stimulation and generally use similar heavy chain V genes compared to WT-
240 stimulated antibodies and display higher convergence (Extended Data Fig. 6a-b). These broad
241 ACE2-competing NAbs in Group A, B and C are also shown to be enriched in individuals who
242 received a booster dose of mRNA vaccines³⁹, which probably accounts for the high plasma
243 neutralizing activity of 3-dose mRNA vaccinees against Omicron variants. Nevertheless, BA.1-
244 stimulated groups B and C NAbs were significantly evaded by BA.4 due to F486V and L452R,
245 concordant with results from DMS (Extended Data Fig. 7a-b), which explains the strong humoral
246 immune evasion ability of BA.4/5.

247 Group D antibodies are most affected by G446S in BA.1, BA.1.1 and BA.3 (Fig. 4d); thus, these
248 NAbs showed higher potency against BA.2 (Fig. 4a-b). However, D1 antibodies showed reduced

249 efficacy against L452 substitutions, with L452M (BA.2.13) causing mild escapes, L452Q causing
250 moderate escapes (BA.2.12.1), and L452R (BA.4/BA.5) causing severe escapes (Fig. 4c-d). In
251 contrast, D2 antibodies, especially those stimulated by BA.1 infection, showed exceptional broad
252 and potent neutralizing activity against all Omicron subvariants, such as LY-CoV1404 (Fig. 4b
253 and Extended Data Fig. 5). Notably, although Group D2 NAbs displayed good breadth, their
254 epitopes are not conserved among sarbecoviruses (Fig. 4d), similar to that of group D1, E2.1, and
255 E2.2. This suggests that their exceptional breadth is possibly due to their rarity in WT and BA.1
256 convalescents (Fig. 3f), and these NAbs may be the next target for SARS-CoV-2 to escape by
257 evolving specific mutations on their epitopes.

258
259 E2 antibodies bind to the chest of RBD³⁵ (Fig. 4a), and their epitopes focus around R346, A348,
260 A352, K356, R357 and I468 (Fig. 4d). Despite similar epitopes, E2.1 antibodies, especially those
261 BA.1-stimulated, display significantly higher neutralizing potency than E2.2 (Fig. 4b). NAbs from
262 the E2 Groups showed good breadth against SARS-COV-2 variants but not against BA.2.12.1 and
263 BA.4/BA.5. L452 substitutions can cause large-scale escapes of E2.1 and E2.2 antibodies (Fig.
264 4c). Similar to the D1 epitope group, L452R and L452Q cause much stronger antibody evasion
265 than L452M (Fig. 4c). Noteworthy, DMS does not reveal the L452 sensitivities of the E2.2 epitope
266 group (Fig. 4d). Together, our results suggest that Omicron may have evolved mutations at L452
267 to specifically evade NAbs from D1 and E2, consequently maximizing Omicron BA.1
268 convalescents' humoral immune evasion. Importantly, Group D1 and E2.1 antibodies also showed
269 decreased efficacy against BA.1.1 compared to BA.1 (Fig. 4b), due to R346K, since both groups
270 of NAbs are sensitive to the R346 substitution (Fig. 4a,d), which shed light on the prevalence of
271 BA.1.1 after BA.1 in the United States.

272

273 **Omicron escapes broad sarbecovirus NAbs**

274 In total, five clusters of antibodies were found to exhibit broad sarbecovirus neutralizing ability
275 with diverse breadth, namely Group E1, E3, F1, F2 and F3 (Extended Data Fig. 4). While Group

276 E3 and F1 antibodies demonstrated weak neutralizing activity against all variants due to their
277 highly conserved binding sites (Extended Data Fig. 8a-c), we found that BA.1-effective E1, F2
278 and F3 NAb, which are rare in WT and Omicron convalescents but enriched in vaccinated SARS
279 convalescents, displayed a systematic reduction in neutralization activity against BA.2 subvariants
280 and BA.3/BA.4/BA.5 (Fig. 2e and 5a-c). This observation explains the sharp NT50 drop of plasma
281 from SARS convalescents against Omicron subvariants other than BA.1 (Fig. 2d). The
282 mechanisms behind the neutralization loss of those broad sarbecovirus antibodies require
283 investigation, which is critical for developing broad-spectrum sarbecovirus vaccines and antibody
284 therapeutics.

285 To study why BA.2 subvariants and BA.3/BA.4/BA.5 could systematically reduce the
286 neutralization efficacy of E1 antibodies, we solved the cryo-EM structures of two BA.1
287 neutralizing E1 antibodies, BD55-3152 and BD55-5840 (SA58), in complex with BA.1 spike
288 proteins using cryo-electron microscopy (cryo-EM) (Fig. 5d and Extended Data Fig. 9a-b). Like
289 S309, E1 antibodies' epitope involves an N-linked glycan on N343 (Fig. 5d). Besides, members
290 of Group E1 are generally sensitive to the changes of G339, E340, T345 and especially R346,
291 revealed by their escaping mutation profiles (Fig. 5h). Intriguingly, the newly acquired mutations
292 of BA.2 do not overlap with the shared epitope of E1 antibodies, suggesting that the systematic
293 reduction in neutralization is not caused by amino-acid substitution, but potentially due to
294 structural alteration. To explore this hypothesis, we further determined the cryo-EM structure of
295 the prefusion-stabilized BA.2 spike in complex with the BD55-5840 Fab (Fig. 5e). A structural
296 comparison with the BA.1 RBD binding to BD55-5840 described above suggests that the 366-377
297 hairpin loop displays significant conformational differences due to S371F and T376A mutations
298 (Fig. 5e and Extended Data Fig. 9d). The overall positions of residues 375-376 have been displaced
299 by >3 Å, which likely further decreases the binding of F2/F3 NAb in addition to the T376A side-
300 chain substitution. As a result, the bulky Phe resulting from the S371F mutation interferes with the
301 positioning of the glycan moiety attached to N343, which in turn budges the heavy chain of BD55-
302 5840 upward. This may explain the reduction of the binding of BD55-5840 and S309, rationalizing

303 their reduced neutralizing activity (Fig. 5a and Extended Data Fig. 9e). Importantly, the N343
304 glycan is critically recognized by almost all E1 neutralizing antibodies, including S309. Thus, this
305 group of broad and potent neutralizing antibodies is likely affected by the S371F mutation in a
306 systematic manner through N343-glycan displacement.

307
308 The epitopes of group F2 and F3 antibodies cover a continuous surface on the backside of RBD
309 and can only bind to the up RBDs (Fig. 2b). To probe how BA.2 escapes antibodies of group F2
310 and F3, we solved the cryo-EM structure of two representative BA.1-effective antibodies in these
311 groups, BD55-1239 from group F2, and BD55-3372 from group F3, in complex with the BA.1 and
312 Delta spike protein respectively (Fig. 5f-g and Extended Data Fig. 9a). Group F2 antibodies can
313 be escaped by RBD mutation involving T376, K378, and R408 (Fig. 5h). Indeed, these residues
314 are all at the heart of BD55-1239's epitope, and are fairly conserved across sarbecoviruses (Fig.
315 5h). Importantly, D405N and R408S harbored by Omicron BA.2 sublineages could alter the
316 antigenic surface that disrupts the binding of F2 antibodies (Fig. 5f), hence completely abolishing
317 the neutralizing capacity of F2 antibodies (Fig. 5b). Similarly, the D405N and R408S mutations
318 harbored by BA.2 subvariants could interrupt the heavy-chain binding of F3 antibodies, causing
319 large-scale escapes of BA.1-effective F3 neutralizing antibodies (Fig. 5c). The above observations
320 were further validated by neutralizing activity against spike-pseudotyped VSV harboring
321 D614G+D405N and D614G+R408S. As expected, Group E1 antibodies were affected by neither
322 D405N nor R408S single substitution, while F2 and F3 antibodies displayed significantly
323 decreased activity (Extended Data Fig. 9c). Nevertheless, several members of F3 antibodies are
324 not sensitive to the D405N and R408S mutations of BA.2, making them good therapeutic drug
325 candidates, such as BD55-5514 (SA55) (Fig. 2e). In sum, we revealed that S371F, D405N and
326 R408S mutations harbored by BA.2 and emerging Omicron variants could induce large-scale
327 escapes of broad sarbecovirus neutralizing antibodies, which is critical to the development of broad
328 sarbecovirus antibody therapeutics and vaccines.

329

330 **BA.1-specific NAbs exhibit poor breadths**

331 Besides the WT/BA.1 cross-reactive NABs, it is also important to investigate the epitope
332 distribution of BA.1-specific NABs that do not react with WT RBD. To do so, we built the yeast
333 display variants library based on RBD BA.1, and determined the escape mutation maps of 102
334 BA.1-specific antibodies. By integrating analysis of the whole dataset containing 1640 SARS-
335 CoV-2 RBD antibodies, we got the embedded features of the BA.1-specific NABs and performed
336 clustering and t-SNE similarly (Fig. 6a). The 102 NABs were clustered into four BA.1-specific
337 epitope groups, named A^{Omi}, B^{Omi}, D^{Omi}, and F3^{Omi}, since these groups are highly related to their
338 corresponding WT epitope groups (Fig. 6a and 6e). These antibodies are all ACE2-competing and
339 display high BA.1 neutralization potency, but cannot neutralize D614G and SARS-CoV-1 (Fig.
340 6b-d), due to N417K/Y501N/H505Y for A^{Omi}, A484E/K478T for B^{Omi}, K440N for D^{Omi}, and
341 R498Q/Y501N for F3^{Omi}, as indicated by average escape maps of each group (Fig. 6e-f). Although
342 some of the previously circulating variants carry the mutations mentioned above, such as N501Y
343 in Alpha, K417N/E484K/N501Y in Beta, and T478K in Delta, only a small subset of the antibodies
344 exhibited neutralizing activity against them (Fig. 6e). Also, nearly all of the BA.1-specific NABs
345 showed poor cross-reactivity against other Omicron subvariants (Fig. 6d). Specifically, most
346 antibodies in F3^{Omi}/A^{Omi} are evaded by BA.2 subvariants and BA.3 possibly due to D405N, and
347 antibodies in B^{Omi} are strongly escaped by BA.4 due to F486V. Some D^{Omi} antibodies might be
348 affected by S446G and were evaded by BA.2 subvariants and BA.4, which were not captured by
349 DMS (Fig. 6g). To further validate the results obtained by DMS, we constructed pseudoviruses
350 based on BA.1 that carry reverting mutations of N417K, K440N, S446G, K478T, A484E, R498Q,
351 Y501N and H505Y, as well as BA.1+D405N and BA.1+R408S. Unfortunately, BA.1+D405N
352 could not generate high enough titers for further experiments despite multiple constructing
353 attempts; thus, we constructed BA.2 + N405D instead. We found that the N417K, R498Q, Y501N
354 and H505Y reversions indeed can lead to heavy evasion of most A^{Omi} and F3^{Omi} antibodies,
355 consistent with DMS results (Fig. 6g). Also, K484E and K478T are the major escaping mutants
356 responsible for the poor breadth of B^{Omi} NABs (Fig. 6d). BA.1+S446G caused a small group of
357 D^{Omi} antibodies to lose neutralization, while R498Q and K440N caused the majority of D^{Omi} NABs
358 not to bind to WT RBD. Importantly, BA.1+R408S did not show neutralization reduction to BA.1-

359 specific NAbs, while BA.2+N405D could restore the neutralization potency of A^{Omi} and F3^{Omi}
360 antibodies against BA.2, indicating that D405N is the main reason that caused their poor cross-
361 reactivity among BA.2/BA.3/BA.4/BA.5 sublineages (Fig. 6d and 6g). Interestingly, these BA.1-
362 specific NAbs displayed different heavy chain V gene usage compared to WT-reactive antibodies
363 in the corresponding epitope group. Specifically, antibodies in A^{Omi} and B^{Omi} did not show
364 significant convergence. IGHV3-53/3-66 only contributes to a small subset of A^{Omi} antibodies.
365 Instead, D^{Omi} antibodies were dominated by IGHV2-70 and IGHV5-51, while IGHV4-59 for F^{Omi}
366 (Extended Data Fig. 10). These three V genes also appeared in WT-reactive antibodies, but were
367 relatively rare and did not show significant epitope enrichment (Extended Data Fig. 6a-b).

368

369 In this study, we showed that Omicron is continuously evolving under immune pressure, and
370 rationalized the appearance of R346K (BA.1.1), L452 substitutions and F486V mutation, which
371 all enabled stronger immune evasion. Unlike when Omicron first appeared, now Omicron
372 sublineages could target the humoral immunity induced by Omicron itself, such as post-
373 vaccination Omicron infection. The Omicron breakthrough infections mainly recall WT-induced
374 memory B cells^{40,41}, which in turn narrows the diversity of antibodies elicited and may further
375 facilitate the appearance of future mutants. These phenomena pose a great challenge to the
376 currently established herd immunity through WT-based vaccination and BA.1/BA.2 infection.
377 Similarly, these also suggest that Omicron BA.1-based vaccine may not be the ideal antigen for
378 inducing broad-spectrum protection against emerging Omicron sublineages.

379

380 Here, by combining high-throughput single-cell sequencing and high-throughput yeast display-
381 based deep mutational screening, we showcased the ability to decipher the complicated humoral
382 immune repertoire elicited by Omicron infection and the underlying immune evasion mechanism
383 of L452 and F486 mutations. The ability to dissect the entire humoral immunity into distinct
384 antibody epitope groups greatly increases the resolution of antibody and mutational escape
385 research. As we have shown, the antibodies in each epitope group show highly concordant
386 attributes and features, largely facilitating the investigation of the immune evasion mechanism of

387 circulating variants. The comprehensive data we provided in this research gives critical
388 instructions to the development of broad-spectrum sarbecovirus vaccines and therapeutic
389 antibodies.
390

ACCELERATED ARTICLE PREVIEW

391 **Figure Legends**

392

393 **Fig. 1 | Structural and receptor-binding characteristics of Omicron subvariants**

394 **a**, Surface representation for structures of S trimer of BA.1, BA.2, BA.3, BA.2.13, BA.2.12.1 and
395 BA.4/5 variants. **b**, Structural interpretation and functional verification for the stability of S protein
396 for BA.1, BA.2, BA.3, BA.2.13, BA.2.12.1 and BA.4/5 variants. The superimposed structures for
397 S protein and the S2 domains of BA.1 (purple), BA.2 (red) and BA.4/5 (blue) are shown on the
398 left. The binding surface areas between S2 subunits of all variants are calculated in the table on
399 the right. **c**, Thermoflour analysis for these Omicron variants. Curves for each Omicron variant are
400 colored in rainbow (BA.1: blue; BA.2: red; BA.3: green; BA.2.13: orange; BA.2.12.1: cyan;
401 BA.4/5: purple). Thermoflour analyses were conducted in biological duplicates. **d**, Binding
402 affinities of RBDs of Omicron variants to hACE2 measured by SPR. SPR analyses were conducted
403 in biological duplicates.

404

405 **Fig. 2 | BA.2.12.1, BA.4 and BA.5 exhibit stronger antibody evasion than BA.2.**

406 **a-d**, Neutralizing titers against SARS-CoV-2 D614G, Omicron subvariants and SARS-CoV-1
407 pseudoviruses in plasma from vaccinated and convalescent individuals. **a**, Individuals who
408 received 3 doses of CoronaVac (n=40). **b**, Individuals who received 2 doses of CoronaVac and 1
409 dose of ZF2001 (n=38). **c**, BA.1 convalescents who had received 3 doses of CoronaVac before
410 infection (n=50). **d**, SARS convalescents who received 2 doses of CoronaVac and 1 dose of
411 ZF2001 (n=28). P-values were calculated using two-tailed Wilcoxon signed-rank tests of paired
412 samples. *, p<0.05; **, p<0.01; ***, p<0.001; n.s., not significant, p>0.05. Geometric mean titers
413 (GMT) are labeled and annotated above each group of points. **e**, Neutralizing activity against
414 SARS-CoV-2 variants and sarbecoviruses by therapeutic neutralizing antibodies; green, IC₅₀ ≤
415 30ng/mL; white, 30ng/mL < IC₅₀ < 1,000ng/mL; red, IC₅₀ ≥ 1,000ng/mL; *, IC₅₀ ≥ 10,000ng/mL.
416 All neutralization assays were conducted in biological duplicates.

417

418 **Fig. 3 | Isolation, characterization, and comprehensive epitope mapping of SARS-CoV-2**
419 **RBD antibodies.**

420 **a**, FACS analysis of pooled memory B cells (IgM⁺/CD27⁺) from BA.1 breakthrough infection
421 convalescents, vaccinated individuals, and BA.1 convalescents without vaccination. **b**, Heavy
422 chain V-domain somatic hypermutation (SHM) rate of BA.1-specific (n=968) and BA.1/WT cross-
423 reactive (n=4782) BCRs obtained from 10X scVDJ-seq from post-vaccination BA.1 infection
424 convalescents. P-value was calculated using two-tailed Wilcoxon rank-sum test. The 25 percentiles,
425 medians and 75 percentiles are shown as boxplots. Kernel density estimation curves of the
426 distribution are shown as violin plots. **c**, t-SNE and unsupervised clustering of SARS-CoV-2
427 wildtype RBD-binding antibodies. 12 epitope groups were identified based on deep mutational
428 scanning of 1538 antibodies. **d-e**, Epitope distribution and projection of antibodies from wildtype
429 convalescents, post-vaccination BA.1 infection convalescents, and vaccinated SARS
430 convalescents. **f**, ACE2 competition level determined by competition ELISA (n=1286) were
431 projected onto the t-SNE. **g**, Neutralizing activity against SARS-CoV-2 D614G (n=1509) and
432 SARS-CoV-1 (HKU-39849, n=1457), respectively. **h**, Average mutational escape score projection

433 of each epitope group on SARS-CoV-2 RBD (PDB: 6M0J). All neutralization assays were
434 conducted in biological duplicates.

435

436 **Fig. 4 | L452 mutants can evade cross-reactive NABs elicited by BA.1 infection**

437 **a**, Epitope of representative antibodies in group D1 (C110, PDB: 7K8V), D2 (LY-CoV1404, PDB:
438 7MMO), E2.1 (BD-744, PDB: 7EY0), and E2.2 (FC08, PDB: 7DX4). Residues highlighted in red
439 indicate mutated sites in Omicron variants. **b**, Neutralizing activity of NABs in group D1 (n=95),
440 D2 (n=53), E2.1 (n=90) and E2.2 (n=161) against spike-pseudotyped SARS-CoV-2 variants.
441 Geometric means of IC50 fold changes compared to BA.2 are annotated above the bars. P-values
442 were calculated using a two-tailed Wilcoxon signed-rank test of paired samples, in comparison to
443 IC50s against BA.2. **c**, Neutralizing activity of representative potent NABs in group D1 (n=24),
444 D2 (n=12), E2.1 (n=23) and E2.2 (n=23) against SARS-CoV-2 L452 mutants. Geometric mean of
445 IC50 fold changes compared to IC50 against D614G are annotated above the points. P-values were
446 calculated using a two-tailed Wilcoxon signed-rank test of paired samples. *, p<0.05; **, p<0.01;
447 ***, p<0.001; n.s., not significant, p>0.05. **d**, Average escape maps at escape hotspots of antibodies
448 in epitope group D1, D2, E2.1 and E2.2, and the corresponding MSA of various sarbecovirus
449 RBDs. Height of each amino acid in the escape maps represents its mutation escape score. Mutated
450 sites in Omicron variants are marked in bold. All neutralization assays were conducted in
451 biological duplicates.

452

453 **Fig. 5 | BA.2 subvariants can escape most broad sarbecovirus neutralizing antibodies**

454 **a-c**, Neutralizing activity against SARS-CoV-1 and SARS-CoV-2 subvariants by NABs in group
455 E1 (**a**, n=70), F2 (**b**, n=171) and F3 (**c**, n=69). Geometric mean of IC50 fold changes compared to
456 BA.2 are annotated above the bars. Geometric means of IC50 are labeled. P-values were calculated
457 using a two-tailed Wilcoxon signed-rank test of paired samples, in comparison to IC50 against
458 BA.2. *, p<0.05; **, p<0.01; ***, p<0.001; n.s., not significant, p>0.05. **d**, Epitope of Group E1
459 antibody BD55-3152 on SARS-CoV-2 BA.1 RBD. **e**, Structural overlay of BD55-5840 in complex
460 of BA.1 and BA.2 RBD. **f-g**, Epitope and interactions on the binding interface of BD55-1239
461 (Group F2) and BD55-3372 (Group F3). Residues of the antibody are blue, and RBD residues are
462 black or red. Residues highlighted in red indicate mutated sites in Omicron variants. **h**, Average
463 escape maps of antibodies in epitope group E1, F2 and F3, and corresponding multiple sequence
464 alignment (MSA) of various sarbecovirus RBDs. Height of each amino acid in the escape maps
465 represents its mutation escape score. Mutated sites in Omicron subvariants are marked in bold. All
466 neutralization assays were conducted in biological duplicates.

467

468 **Fig. 6 | BA.1-specific antibodies elicited by BA.1 infection exhibit poor breadth**

469 **a**, Four epitope groups were identified among 102 BA.1-specific NABs, via k-means clustering
470 and t-SNE of BA.1-RBD-based DMS profiles. **b-c**, Distribution of ACE2 competition level and
471 neutralizing activities against BA.1. **d**, Pseudovirus neutralizing activities of BA.1-specific
472 antibodies against SARS-CoV-1 and SARS-CoV-2 variants (A^{Omi}, n=18; B^{Omi}, n=30; D^{Omi}, n=22;
473 F3^{Omi}, n=32). Geometric mean of IC50 fold changes compared to IC50 against BA.1 are annotated
474 above the bars. Geometric means of IC50 are labeled. **e**, Average mutational escape score

475 projection of each BA.1-specific epitope group on SARS-CoV-2 RBD (PDB: 7WPB). **f**, Averaged
476 escape maps at escape hotspots of the 102 NAb in four epitope groups, and corresponding MSA
477 of various sarbecovirus RBDs. Height of each amino acid in the escape maps represents its
478 mutation escape score. Mutated sites in Omicron variants are marked in bold. WT-related escaping
479 mutations are highlighted. **g**, Neutralizing activities of BA.1-specific NAb against BA.1 or BA.2
480 based pseudoviruses carrying single substitution (A^{Omi}, n=18; B^{Omi}, n=30; D^{Omi}, n=22; F3^{Omi},
481 n=32).. Geometric mean of IC50 fold changes compared to IC50 against BA.1 are annotated above
482 the bars. All P-values were calculated using a two-tailed Wilcoxon signed-rank test of paired
483 samples, in comparison with BA.1 IC50. *, p<0.05; **, p<0.01; ***, p<0.001; n.s., not significant,
484 p>0.05. All neutralization assays were conducted in biological duplicates.

485

486 References

- 487 1 Chen, C. *et al.* CoV-Spectrum: analysis of globally shared SARS-CoV-2 data to identify and characterize
488 new variants. *Bioinformatics* **38**, 1735-1737, doi:10.1093/bioinformatics/btab856 (2021).
- 489 2 Greaney, A. J. *et al.* Complete Mapping of Mutations to the SARS-CoV-2 Spike Receptor-Binding Domain
490 that Escape Antibody Recognition. *Cell Host Microbe* **29**, 44-57 e49, doi:10.1016/j.chom.2020.11.007 (2021).
- 491 3 Cao, Y. *et al.* Omicron escapes the majority of existing SARS-CoV-2 neutralizing antibodies. *Nature* **602**,
492 657-663, doi:10.1038/s41586-021-04385-3 (2022).
- 493 4 Westendorf, K. *et al.* LY-CoV1404 (bebtelovimab) potently neutralizes SARS-CoV-2 variants. *Cell Reports*
494 **39**, 110812, doi:<https://doi.org/10.1016/j.celrep.2022.110812> (2022).
- 495 5 Zost, S. J. *et al.* Potently neutralizing and protective human antibodies against SARS-CoV-2. *Nature* **584**,
496 443-449, doi:10.1038/s41586-020-2548-6 (2020).
- 497 6 Cele, S. *et al.* Omicron extensively but incompletely escapes Pfizer BNT162b2 neutralization. *Nature* **602**,
498 654-656, doi:10.1038/s41586-021-04387-1 (2022).
- 499 7 Collie, S., Champion, J., Moultrie, H., Bekker, L.-G. & Gray, G. Effectiveness of BNT162b2 Vaccine against
500 Omicron Variant in South Africa. *New England Journal of Medicine* **386**, 494-496,
501 doi:10.1056/NEJMc2119270 (2021).
- 502 8 Lu, L. *et al.* Neutralization of SARS-CoV-2 Omicron variant by sera from BNT162b2 or Coronavac vaccine
503 recipients. *Clin Infect Dis*, ciab1041, doi:10.1093/cid/ciab1041 (2021).
- 504 9 Bruel, T. *et al.* Serum neutralization of SARS-CoV-2 Omicron sublineages BA.1 and BA.2 in patients
505 receiving monoclonal antibodies. *Nat Med*, doi:10.1038/s41591-022-01792-5 (2022).
- 506 10 Cameroni, E. *et al.* Broadly neutralizing antibodies overcome SARS-CoV-2 Omicron antigenic shift. *Nature*
507 **602**, 664-670, doi:10.1038/s41586-021-04386-2 (2022).
- 508 11 Dejnirattisai, W. *et al.* SARS-CoV-2 Omicron-B.1.1.529 leads to widespread escape from neutralizing
509 antibody responses. *Cell* **185**, 467-484 e415, doi:10.1016/j.cell.2021.12.046 (2022).
- 510 12 Liu, L. *et al.* Striking antibody evasion manifested by the Omicron variant of SARS-CoV-2. *Nature* **602**, 676-
511 681, doi:10.1038/s41586-021-04388-0 (2022).
- 512 13 Planas, D. *et al.* Considerable escape of SARS-CoV-2 Omicron to antibody neutralization. *Nature* **602**, 671-
513 675, doi:10.1038/s41586-021-04389-z (2022).
- 514 14 Hsieh, C.-L. *et al.* Structure-based design of prefusion-stabilized SARS-CoV-2 spikes. *Science* **369**, 1501-
515 1505, doi:doi:10.1126/science.abd0826 (2020).

- 516 15 Du, S. *et al.* Structurally Resolved SARS-CoV-2 Antibody Shows High Efficacy in Severely Infected
517 Hamsters and Provides a Potent Cocktail Pairing Strategy. *Cell* **183**, 1013-1023 e1013,
518 doi:10.1016/j.cell.2020.09.035 (2020).
- 519 16 Cui, Z. *et al.* Structural and functional characterizations of infectivity and immune evasion of SARS-CoV-2
520 Omicron. *Cell* **185**, 860-871 e813, doi:10.1016/j.cell.2022.01.019 (2022).
- 521 17 Starr, T. N. *et al.* Deep Mutational Scanning of SARS-CoV-2 Receptor Binding Domain Reveals Constraints
522 on Folding and ACE2 Binding. *Cell* **182**, 1295-1310 e1220, doi:10.1016/j.cell.2020.08.012 (2020).
- 523 18 Wang, Q. *et al.* SARS-CoV-2 Omicron BA.2.12.1, BA.4, and BA.5 subvariants evolved to extend antibody
524 evasion. *bioRxiv*, 2022.2005.2026.493517, doi:10.1101/2022.05.26.493517 (2022).
- 525 19 Tuekprakhon, A. *et al.* Further antibody escape by Omicron BA.4 and BA.5 from vaccine and BA.1 serum.
526 *bioRxiv*, 2022.2005.2021.492554, doi:10.1101/2022.05.21.492554 (2022).
- 527 20 Iketani, S. *et al.* Antibody evasion properties of SARS-CoV-2 Omicron sublineages. *Nature*,
528 doi:10.1038/s41586-022-04594-4 (2022).
- 529 21 Yamasoba, D. *et al.* Virological characteristics of SARS-CoV-2 BA.2 variant. *bioRxiv*,
530 2022.2002.2014.480335, doi:10.1101/2022.02.14.480335 (2022).
- 531 22 Tan, C. W. *et al.* Pan-Sarbecovirus Neutralizing Antibodies in BNT162b2-Immunized SARS-CoV-1
532 Survivors. *N Engl J Med* **385**, 1401-1406, doi:10.1056/NEJMoa2108453 (2021).
- 533 23 Hansen, J. *et al.* Studies in humanized mice and convalescent humans yield a SARS-CoV-2 antibody cocktail.
534 *Science* **369**, 1010-1014, doi:10.1126/science.abd0827 (2020).
- 535 24 Shi, R. *et al.* A human neutralizing antibody targets the receptor-binding site of SARS-CoV-2. *Nature* **584**,
536 120-124, doi:10.1038/s41586-020-2381-y (2020).
- 537 25 Jones, B. E. *et al.* The neutralizing antibody, LY-CoV555, protects against SARS-CoV-2 infection in
538 nonhuman primates. *Sci Transl Med* **13**, eabf1906, doi:10.1126/scitranslmed.abf1906 (2021).
- 539 26 Ju, B. *et al.* Human neutralizing antibodies elicited by SARS-CoV-2 infection. *Nature* **584**, 115-119,
540 doi:10.1038/s41586-020-2380-z (2020).
- 541 27 Cao, Y. *et al.* Potent Neutralizing Antibodies against SARS-CoV-2 Identified by High-Throughput Single-
542 Cell Sequencing of Convalescent Patients' B Cells. *Cell* **182**, 73-84 e16, doi:10.1016/j.cell.2020.05.025
543 (2020).
- 544 28 Rappazzo, C. G. *et al.* Broad and potent activity against SARS-like viruses by an engineered human
545 monoclonal antibody. *Science* **371**, 823-829, doi:10.1126/science.abf4830 (2021).
- 546 29 Pinto, D. *et al.* Cross-neutralization of SARS-CoV-2 by a human monoclonal SARS-CoV antibody. *Nature*
547 **583**, 290-295, doi:10.1038/s41586-020-2349-y (2020).
- 548 30 Park, Y. J. *et al.* Antibody-mediated broad sarbecovirus neutralization through ACE2 molecular mimicry.
549 *Science* **375**, 449-454, doi:10.1126/science.abm8143 (2022).
- 550 31 Cao, Y. *et al.* Humoral immune response to circulating SARS-CoV-2 variants elicited by inactivated and
551 RBD-subunit vaccines. *Cell Res* **31**, 732-741, doi:10.1038/s41422-021-00514-9 (2021).
- 552 32 Starr, T. N. *et al.* SARS-CoV-2 RBD antibodies that maximize breadth and resistance to escape. *Nature*,
553 doi:10.1038/s41586-021-03807-6 (2021).
- 554 33 Greaney, A. J. *et al.* Mapping mutations to the SARS-CoV-2 RBD that escape binding by different classes of
555 antibodies. *Nature Communications* **12**, 4196, doi:10.1038/s41467-021-24435-8 (2021).
- 556 34 Corti, D., Purcell, L. A., Snell, G. & Veessler, D. Tackling COVID-19 with neutralizing monoclonal antibodies.
557 *Cell* **184**, 3086-3108, doi:10.1016/j.cell.2021.05.005 (2021).

- 558 35 Dejnirattisai, W. *et al.* The antigenic anatomy of SARS-CoV-2 receptor binding domain. *Cell* **184**, 2183-2200
559 e2122, doi:10.1016/j.cell.2021.02.032 (2021).
- 560 36 Piccoli, L. *et al.* Mapping Neutralizing and Immunodominant Sites on the SARS-CoV-2 Spike Receptor-
561 Binding Domain by Structure-Guided High-Resolution Serology. *Cell* **183**, 1024-1042 e1021,
562 doi:10.1016/j.cell.2020.09.037 (2020).
- 563 37 Barnes, C. O. *et al.* SARS-CoV-2 neutralizing antibody structures inform therapeutic strategies. *Nature* **588**,
564 682-687, doi:10.1038/s41586-020-2852-1 (2020).
- 565 38 Yuan, M. *et al.* Structural and functional ramifications of antigenic drift in recent SARS-CoV-2 variants.
566 *Science* **373**, 818-823, doi:10.1126/science.abh1139 (2021).
- 567 39 Muecksch, F. *et al.* Increased Memory B Cell Potency and Breadth After a SARS-CoV-2 mRNA Boost.
568 *Nature*, doi:10.1038/s41586-022-04778-y (2022).
- 569 40 Quandt, J. *et al.* Omicron BA.1 breakthrough infection drives cross-variant neutralization and memory B cell
570 formation against conserved epitopes. *Science Immunology* **0**, eabq2427,
571 doi:doi:10.1126/sciimmunol.abq2427 (2022).
- 572 41 Park, Y.-J. *et al.* Imprinted antibody responses against SARS-CoV-2 Omicron sublineages. *bioRxiv*,
573 2022.2005.2008.491108, doi:10.1101/2022.05.08.491108 (2022).

574

575 **Methods**

576 **Plasma and PBMC isolation**

577 Blood samples were obtained from 40 volunteers who received 3 doses of CoronaVac, 39
578 individuals who received 2 doses of CoronaVac and 1 booster dose of ZF2001, 54 BA.1
579 convalescents who had received 3 doses of CoronaVac before BA.1 infection^{42,43}, and 30 SARS
580 convalescents who received 2 doses of CoronaVac and 1 dose of ZF2001. The volunteers' blood
581 samples were obtained 4 weeks after the booster shot or 4 weeks after discharge from the hospital
582 after BA.1 infection. COVID-19 disease severity was defined as asymptomatic, mild, moderate,
583 severe and critical according to WHO living guidance for clinical management of COVID-19⁴⁴.
584 Relevant experiments regarding SARS convalescents and SARS-CoV-2 vaccinees were approved
585 by the Beijing Ditan Hospital Capital Medical University (Ethics committee archiving No. LL-
586 2021-024-02), the Tianjin Municipal Health Commission, and the Ethics Committee of Tianjin
587 First Central Hospital (Ethics committee archiving No. 2022N045KY). Written informed consent
588 was obtained from each participant in accordance with the Declaration of Helsinki. All participants
589 provided written informed consent for the collection of information, storage and usage of their
590 clinical samples for research purpose, and publication of data generated from this study.

591 Whole blood samples were mixed and subjected to Ficoll (Cytiva, 17-1440-03) gradient
592 centrifugation after 1:1 dilution in PBS+2% FBS to isolate plasma and peripheral blood
593 mononuclear cells (PBMC). After centrifugation, plasma was collected from upper layer and cells
594 were harvested at the interface, respectively. PBMCs were further prepared through centrifugation,
595 red blood cells lysis (Invitrogen™ eBioscience™ 1X RBC Lysis Buffer, 00-4333-57) and
596 washing steps. Samples were stored in FBS (Gibco) with 10% DMSO (Sigma) in liquid nitrogen
597 if not used for downstream process immediately. Cryopreserved PBMCs were thawed in
598 DPBS+2% FBS (Stemcell, 07905).

599

600 **Antibody isolation and recombinant production**

601 SARS-CoV-1 and SARS-CoV-2 RBD cross-binding memory B cells were isolated from PBMC
602 of SARS convalescents who received SARS-CoV-2 vaccine and BA.1 infected convalescents who
603 had been vaccinated against COVID-19 prior to infection. Briefly, CD19⁺ B cells were isolated
604 from PBMC with EasySep Human CD19 Positive Selection Kit II (STEMCELL, 17854). Every
605 10⁶ B cells in 100 μL were then stained with 2.5 μL FITC anti-human CD19 antibody
606 (BioLegend, 392508), 2.5 μL FITC anti-human CD20 antibody (BioLegend, 302304), 3.5 μL
607 Brilliant Violet 421 anti-human CD27 antibody (BioLegend, 302824), 3 μL PE/Cyanine7 anti-
608 human IgM antibody (BioLegend, 314532), 0.0052 μg biotinylated Ovalbumin (SinoBiological)
609 conjugated with Brilliant Violet 605 Streptavidin (BioLegend, 405229), 0.0032 μg SARS-CoV-1
610 biotinylated RBD protein (His & AVI Tag) (SinoBiological, 40634-V27H-B) conjugated with PE-
611 streptavidin (BioLegend, 405204), 0.0032 μg SARS-CoV-2 biotinylated RBD protein (His & AVI
612 Tag) (SinoBiological, 40592-V27H-B) conjugated with APC-streptavidin (BioLegend, 405207),
613 and 5 μL 7-AAD (Invitrogen, 00-6993-50). 7-AAD⁻, CD19/CD20⁺, CD27⁺, IgM⁻, OVA⁻, SARS-
614 COV-1 RBD⁺, and SARS-CoV-2 RBD⁺ were sorted with MoFlo Astrios EQ Cell Sorter
615 (Beckman Coulter).

616 SARS-CoV-2 BA.1 RBD binding memory B cells were isolated from BA.1 infected convalescents
617 who received SARS-CoV-2. Briefly, CD19⁺ B cells were isolated with EasySep Human CD19

618 Positive Selection Kit II. Every 10^6 B cells in 100 μ L solution were then stained with 3 μ L FITC
619 anti-human CD20 antibody (BioLegend, 302304), 3.5 μ L Brilliant Violet 421 anti-human CD27
620 antibody (BioLegend, 302824), 2 μ L PE/Cyanine7 anti-human IgM antibody (BioLegend,
621 314532), 2 μ L PE/Cyanine7 anti-human IgD antibody (BioLegend, 348210), 0.0032 μ g
622 biotinylated SARS-CoV-2 BA.1 protein (His & AVI Tag) (SinoBiological, 40592-V49H7-B)
623 conjugated with PE-streptavidin or APC-streptavidin (TotalSeq-C0971 Streptavidin, BioLegend,
624 405271 and TotalSeq-C0972 Streptavidin, BioLegend, 405273), 0.0032 μ g SARS-CoV-2 WT
625 biotinylated RBD protein (His & AVI Tag) conjugated with Brilliant Violet 605 Streptavidin and
626 TotalSeq-C0973 Streptavidin (BioLegend, 405275) and TotalSeq-C0974 Streptavidin (BioLegend,
627 405277), 0.0052 μ g biotinylated Ovalbumin conjugated with TotalSeq-C0975 Streptavidin
628 (BioLegend, 405279) and 5 μ L 7-AAD (Invitrogen, 00-6993-50). 7-AAD-, CD20+, CD27+, IgM-,
629 IgD-, SARS-CoV-2 BA.1 RBD+ were sorted with MoFlo Astrios EQ Cell Sorter. FACS data were
630 analyzed using FlowJo v10.8 (BD Biosciences).

631 Sorted B cells were then processed with Chromium Next GEM Single Cell V(D)J Reagent Kits
632 v1.1 following the manufacturer's user guide (10x Genomics, CG000208). Briefly, Cells sorted
633 were resuspended in PBS after centrifugation. Gel beads-in-emulsion (GEMs) were obtained with
634 10X Chromium controller and then subjected to reverse transcription (RT). After GEM-RT clean
635 up, RT products were subject to preamplification. After amplification and purification with
636 SPRIselect Reagent Kit (Beckman Coulter, B23318) of RT products, B cell receptor (BCR)
637 sequence (paired V(D)J) were enriched with 10X BCR primers. After library preparation, libraries
638 were sequenced by Novaseq 6000 platform running Novaseq 6000 S4 Reagent Kit v1.5 300 cycles
639 (Illumina, 20028312) or NovaSeq XP 4-Lane Kit v1.5 (Illumina, 20043131).

640 **B cell RNA and feature barcode data analysis**

641 Using Cell Ranger (v6.1.1) pipeline, the mRNA fastq reads were processed and aligned to the
642 human GRCh38 genome for gene expression profile. Genes expressed in less than 10 cells and
643 cells expressed less than 100 genes or high-level mitochondria genes were removed, to filter out

644 low-quality data. Raw counts were normalized and scaled with Seurat⁴⁵ (v 4.0.3), while principal
645 components analysis (PCA) and uniform manifold approximation and projection (UMAP) were
646 performed for cluster and visualization. Cell types were identified using SingleR⁴⁶ (v1.6.1) with
647 Monaco human immune reference⁴⁷. Feature barcode reads were also counted by Cell Ranger
648 (v6.1.1) as antibody capture library, and a cell was considered to bind the corresponding antigen
649 of dominant feature barcodes (>25% in this cell).

650 **Antibody sequence analysis**

651 The antibody sequences obtained from 10X Genomics V(D)J sequencing were aligned to GRCh38
652 reference and assembled as immunoglobulin contigs by the Cell Ranger (v6.1.1) pipeline. Non-
653 productive contigs and B cells that had multiple heavy chain or light chain contigs were filtered
654 out of the analysis. V(D)J gene annotation was performed using NCBI IgBlast (v1.17.1) with the
655 IMGT reference. Mutations on V(D)J nucleotide sequences were calculated by using the
656 igpipeline, which compared the sequences to the closest germline genes and counted the number
657 of different nucleotides. For antibodies from public sources whose original sequencing nucleotide
658 sequences were not all accessible, the antibody amino acid sequences were annotated by
659 IMGT/DomainGapAlign⁴⁸ (v4.10.2) with default parameters. The V-J pairs were visualized by R
660 package circize (v0.4.10).

661 **Deep Mutational Scanning Library construction**

662 Deep mutational scanning libraries were constructed as previously described³. Briefly, SARS-
663 CoV-2 RBD mutant libraries were constructed from Wuhan-Hu-1 RBD sequence (GenBank:
664 MN908947, residues N331-T531), and Omicron RBD mutant libraries were created in a similar
665 way based on Wuhan-Hu-1 RBD sequence with the addition of G339D, S371L, S373P, S375F,
666 K417N, N440K, G446S, S477N, T478K, E484A, Q493R, G496S, Q498R, N501Y, and Y505H
667 mutations. Duplicated libraries were independently produced, theoretically containing 3819
668 possible amino acid mutations. Each RBD mutant was barcoded with a unique 26-nucleotide (N26)

669 sequence and Pacbio sequencing was used to identify the correspondence of RBD mutant and N26
670 barcode. After mutant library transformation, ACE2 binders were enriched for downstream
671 mutation profile experiment.

672 **High-throughput antibody-escape mutation profiling**

673 The previously described high-throughput MACS (magnetic-activated cell sorting)-based
674 antibody-escape mutation profiling system^{3,17} was used to characterize mutation escape profile for
675 neutralizing antibodies. Briefly, ACE2 binding mutants were induced overnight for RBD
676 expression and washed followed by two rounds of Protein A antibody based negative selection
677 and MYC-tag based positive selection to enrich RBD expressing cells. Protein A antibody
678 conjugated products were prepared following the protocol of Dynabeads Protein A (Thermo
679 Fisher, 10008D) and incubated with induced yeast libraries at room temperature for 30min with
680 shaking. MYC-tag based positive selection was performed according to the manufacturer's
681 instructions (Thermo Fisher, 88843).

682 After three rounds of sequential cell sorting, the obtained cells were recovered overnight. Plasmids
683 were extracted from pre- and post-sort yeast populations by 96-Well Plate Yeast Plasmid Preps
684 Kit (Coolaber, PE053). The extracted plasmids were then used to amplify N26 barcode sequences
685 by PCR. The final PCR products were purified with 1X AMPure XP magnetic beads (Beckman
686 Coulter, A63882) and submitted to 75bp single-end sequencing at Illumina Nextseq 500 platform.

687 **Processing of deep mutational scanning data**

688 Single-end Illumina sequencing reads were processed as previously described. Briefly, reads were
689 trimmed into 16 or 26 bp and aligned to the reference barcode-variant dictionary with dms_variants
690 package (v0.8.9). Escape scores of variants were calculated as $F \times (n_{X,ab} / N_{ab}) / (n_{X,ref} / N_{ref})$, where
691 $n_{X,ab}$ and $n_{X,ref}$ is the number of reads representing variant X, and N_{ab} and N_{ref} are the total number
692 of valid reads in antibody-selected (ab) and reference (ref) library, respectively. F is a scale factor
693 defined as the 99th percentiles of escape fraction ratios. Variants detected by less than 6 reads in

694 the reference library were removed to avoid sampling noise. Variants containing mutations with
695 ACE2 binding below -2.35 or RBD expression below -1 were removed as well, according to data
696 previously reported. For RBD^{BA.1}-based libraries, due to the lack of corresponding ACE2 binding
697 and RBD expression data, we used the RBD expression of RBD^{Beta}-based DMS as filter instead⁴⁹,
698 and did not perform the ACE2-binding filter. Mutations on residues that use different amino acids
699 in Beta and BA.1 are not filtered, except R493P, S496P, R498P, H505P and all mutations on F375,
700 which were excluded in the analysis due to low expression. Finally, global epistasis models were
701 built using dms_variants package to estimate mutation escape scores. For most antibodies, at least
702 two independent assays are conducted and single mutation escape scores are averaged across all
703 experiments that pass quality control.

704

705 **Antibody clustering and visualization**

706 Site total escape scores, defined as the sum of escape scores of all mutations at a particular site on
707 RBD, were used to evaluate the impact of mutations on each site for each antibody. Each of these
708 scores is considered as a feature of a certain antibody and used to construct a feature matrix $\mathbf{A}_{N \times M}$
709 for downstream analysis, where N is the number of antibodies and M is the number of features
710 (valid sites). Informative sites were selected using sklearn.feature_selection.VarianceThreshold of
711 scikit-learn Python package (v0.24.2) with the variance threshold as 0.1. Then, the selected
712 features were L2-normalized across antibodies using sklearn.preprocessing.normalize. The
713 resulting matrix is referred as $\mathbf{A}'_{N \times M'}$, where M' is the number of selected features. The
714 dissimilarity of two antibodies i, j is defined as $1 - \text{Corr}(\mathbf{A}'_i, \mathbf{A}'_j)$, where $\text{Corr}(\mathbf{x}, \mathbf{y})$ is the Pearson's
715 correlation coefficient of vector \mathbf{x} and \mathbf{y} . We used sklearn.manifold.MDS to reduce the number of
716 features from M' to $D=20$ with multidimensional scaling under the above metric. Antibodies are
717 clustered into 12 epitope groups using sklearn.cluster.KMeans of scikit-learn in the resulting D -
718 dimensional feature space. Finally, these D -dimensional representations of antibodies were further
719 embedded into two-dimensional space for visualization with t-SNE using sklearn.manifold.TSNE
720 of scikit-learn. For the 102 BA.1-specific antibodies that were assayed with RBD^{BA.1}-based yeast
721 display library, the 20-dimensional embedding were generated using MDS with all 1640

722 antibodies' DMS profile, but clustering and t-SNE were conducted independently. To project these
723 antibodies onto the t-SNE space of 1538 antibodies assayed by RBD^{WT}-based DMS, we calculated
724 the pairwise Euclidean distance between 102 antibodies using RBD^{BA.1}-based DMS and 1538
725 antibodies using RBD^{WT}-based DMS in the 20-dimensional MDS space. The position of each
726 BA.1-specific antibody in the original t-SNE space is defined as the average position of its ten
727 nearest antibodies using RBD^{WT}-based DMS. All t-SNE plots were generated by R package
728 ggplot2 (v3.3.3).

729

730 **Pseudovirus neutralization assay**

731 SARS-CoV-2 spike (GenBank: MN908947), Pangolin-GD spike (GISAID: EPI_ISL_410721),
732 RaTG13 spike (GISAID: EPI_ISL_402131), SARS-CoV-1 spike (GenBank: AY278491),
733 Omicron BA.1 spike (A67V, H69del, V70del, T95I, G142D, V143del, Y144del, Y145del,
734 N211del, L212I, ins214EPE, G339D, S371L, S373P, S375F, K417N, N440K, G446S, S477N,
735 T478K, E484A, Q493R, G496S, Q498R, N501Y, Y505H, T547K, D614G, H655Y, N679K,
736 P681H, N764K, D796Y, N856K, Q954H, N969K, L981F), BA.2 spike (GISAID:
737 EPI_ISL_7580387, T19I, L24S, del25-27, G142D, V213G, G339D, S371F, S373P, S375F,
738 T376A, D405N, R408S, K417N, N440K, G446S, S477N, T478K, E484A, Q493R, Q498R,
739 N501Y, Y505H, D614G, H655Y, N679K, P681H, N764K, D796Y, Q954H, N969K), BA.1.1
740 spike (BA.1+R346K), BA.3 spike (A67V, del69-70, T95I, G142D, V143del, Y144del, Y145del,
741 N211del, L212I, G339D, S371F, S373P, S375F, D405N, K417N, N440K, G446S, S477N, T478K,
742 E484A, Q493R, Q498R, N501Y, Y505H, D614G, H655Y, N679K, P681H, N764K, D796Y,
743 Q954H, N969K), BA.2.12.1 spike (BA.2+L452Q+S704L), BA.2.13 spike (BA.2+L452M), BA.4
744 spike (T19I, L24S, del25-27, del69-70, G142D, V213G, G339D, S371F, S373P, S375F, T376A,
745 D405N, R408S, K417N, N440K, G446S, L452R, S477N, T478K, E484A, F486V, Q498R,
746 N501Y, Y505H, D614G, H655Y, N679K, P681H, N764K, D796Y, Q954H, N969K) plasmid is
747 constructed into pcDNA3.1 vector. G*ΔG-VSV virus (VSV G pseudotyped virus, Kerafast) is
748 used to infect 293T cells (American Type Culture Collection [ATCC], CRL-3216), and spike

749 protein expressing plasmid was used for transfection at the same time. After culture, the
750 supernatant containing pseudovirus was harvested, filtered, aliquoted, and frozen at -80°C for
751 further use.

752 Pseudovirus detection of Pangolin-GD and RaTG13 was performed in 293T cells overexpressing
753 human angiotensin-converting enzyme 2 (293T-hACE2 cells). Other pseudovirus neutralization
754 assays were performed using the Huh-7 cell line (Japanese Collection of Research Bioresources
755 [JCRB], 0403).

756 Monoclonal antibodies or plasma were serially diluted (5-fold or 3-fold) in DMEM (Hyclone,
757 SH30243.01) and mixed with pseudovirus in 96-well plates. After incubation at 5% CO_2 and 37°C
758 for 1 h, digested Huh-7 cell (Japanese Collection of Research Bioresources [JCRB], 0403) or
759 293T-hACE2 cells (AmericanTypeCultureCollection[ATCC],CRL-3216) were seeded. After 24
760 hours of culture, supernatant was discarded and D-luciferin reagent (PerkinElmer, 6066769) was
761 added to react in the dark, and the luminescence value was detected using a microplate
762 spectrophotometer (PerkinElmer, HH3400). IC_{50} was determined by a four-parameter logistic
763 regression model using PRISM (versions 9.0.1).

764 **ELISA**

765 To detect the broad-spectrum binding of the antibodies among Sarbecovirus, we entrusted
766 SinoBiological Technology Co., Ltd. to synthesize a panel of 20 sarbecovirus RBDs
767 (Supplementary Table 3). According to the sequence of 20 RBDs, a set of nested primers was
768 designed. The coding sequences were obtained by the overlap-PCR with a 6xHis tag sequence to
769 facilitate protein purification. The purified PCR products were ligated to the secretory expression
770 vector pCMV3 with CMV promoter, and then transformed into *E. coli* competent cells XL1-blue.
771 Monoclones with correct transformation were cultured and expanded, and plasmids were
772 extracted. Healthy HEK293F cells were passaged into a new cell culture and grown in suspension
773 at 37°C , 120 RPM, 8% CO_2 to logarithmic growth phase and transfected with the recombinant
774 constructs by using liposomal vesicles as DNA carrier. After transfection, the cell cultures were

775 followed to assess the kinetics of cell growth and viability for 7 days. The cell expression
776 supernatant was collected, and after centrifugation, passed through a Ni column for affinity
777 purification. The molecular size and purity of eluted protein was confirmed by SDS-PAGE.
778 Production lot numbers and concentration information of the 20 Sarbecovirus proteins are shown
779 in Supplementary Table 4. The WT RBD in the article is SARS-CoV-2 (2019-nCoV) Spike RBD-
780 His Recombinant Protein (SinoBiological, 40592-V08H).

781
782 A panel of 21 sarbecovirus RBDs (Supplementary Table 3) in PBS was pre-coated onto ELISA
783 Plates (NEST, 514201) at 4°C overnight. The plates were washed and blocked. Then 1µg/ml
784 purified antibodies or serially diluted antibodies were added and incubated at room temperature
785 (RT) for 20min. Next, Peroxidase-conjugated AffiniPure Goat Anti-Human IgG (H+L)
786 (JACKSON, 109-035-003) was applied and incubated at RT for 15min. Tetramethylbenzidine
787 (TMB) (Solarbio, 54827-17-7) was added onto the plates. The reaction was terminated by 2 M
788 H₂SO₄ after 10min incubation. Absorbance was measured at 450 nm using Ensign Multimode
789 Plate Reader (PerkinElmer, HH3400). ELISA OD450 measurements at different antibody
790 concentration for a particular antibody-antigen pair are fit to the model $y=Ac^n/(c^n + E^n)$ using R
791 package mosaic (v1.8.3), where y is OD450 values and c is corresponding antibody concentration.
792 A , E , n are parameters, where E is the desired EC₅₀ value for the specific antibody and antigen.

793

794 **Antibody-ACE2 competition for RBD**

795 Omicron-RBD (Sino Biological, 40592-V08H121) protein in PBS was immobilized on the ELISA
796 plates at 4°C overnight. The coating solution was removed and washed three times by PBST and
797 the plates were then blocked for 2 h. After blocking, the plates were washed five times, and the
798 mixture of ACE2-biotin (Sino Biological, 10108-H27B-B) and serially diluted competitor
799 antibodies was added followed by 30min incubation at RT. Then Peroxidase-conjugated
800 Streptavidin (Jackson ImmunoResearch, 016-030-084) was added into each well for another
801 20min incubation at RT. After washing the plates for five times, Tetramethylbenzidine (TMB)
802 (Solarbio, 54827-17-7) was added into each well. After 10 min, the reaction was terminated by

803 2M H₂SO₄. Absorbance was measured at 450 nm using Ensign Multimode Plate Reader
804 (PerkinElmer, HH3400). The ACE2 competition coefficient is calculated as (B-A)/B, where B is
805 the OD450 value under 0.3ug/ml antibody concentration and A is the OD450 value under 6ug/ml
806 antibody concentration.

807

808 **Biolayer Interferometry**

809 Biolayer interferometry assays were performed on Octet® RED 384 Protein Analysis System
810 (Fortebio) according to the manufacturer's instruction. To measure the binding affinities,
811 monoclonal antibodies were immobilized onto Protein A biosensors (Fortebio) and the fourfold
812 serial dilutions of Omicron S trimer (BA.1 and BA.2) in PBS were used as analytes. Data were
813 collected with Octet Acquisition 9.0 (Fortebio) and analyzed by Octet Analysis 9.0 (Fortebio) and
814 Octet Analysis Studio 12.2 (Fortebio).

815

816 **S trimer thermal stability assay**

817 The thermal stability assay was performed to detect the exposed hydrophobic residues by an
818 MX3005 qPCR instrument (Agilent, Santa Clara, USA) with SYPRO Red (Invitrogen, Carlsbad,
819 USA) as fluorescent probes. Here, we set up 25 µL reaction system (pH=8.0) which contained 5 µg
820 of target protein (S trimer of Omicron lineage), 1000x SYPRO Red, and ramped up the temperature
821 from 25°C to 99°C. Fluorescence was recorded in triplicate at an interval of 1°C.

822

823 **Surface plasmon resonance**

824 Human ACE2 was immobilized onto CM5 sensor chips using a Biacore 8K (GE Healthcare).
825 Serial dilutions of purified S trimer or RBD of Omicron lineages were injected, ranging in
826 concentrations from 100 to 6.25 nM. The response units were recorded at room temperature using
827 Biacore 8K Evaluation Software (v3.0.12.15655; GE Healthcare), and the resulting data were

828 fitted to a 1:1 binding model using BIAcore 8K Evaluation Software (v3.0.12.15655; GE
829 Healthcare).

830

831 **Protein expression and purification for cryo-EM study**

832 The S6P expression construct encoding the SARS-CoV-2 spike ectodomain (residues 1-1208) with
833 six stabilizing Pro substitutions (F817P, A892P, A899P, A942P, K986P, and V987P) and a
834 “GSAS” substitution for the furin cleavage site (residues 682–685) was previously described¹⁵.

835 The Delta specific mutations (T19R, G142D, 156del, 157del, R158G, L452R, T478K, D614G,
836 P681R, D950N) were introduced into this construct using site-directed mutagenesis. The S6P

837 expression construct containing the Omicron BA.1 mutations (A67V, H69del, V70del, T95I,
838 G142D, V143del, Y144del, Y145del, N211del, L212I, ins214EPE, G339D, S371L, S373P,

839 S375F, K417N, N440K, G446S, S477N, T478K, E484A, Q493R, G496S, Q498R, N501Y,
840 Y505H, T547K, D614G, H655Y, N679K, P681H, N764K, D796Y, N856K, Q954H, N969K,

841 L981F) were assembled from three synthesized DNA fragments. The S6P expression construct
842 containing the Omicron BA.2 mutations (T19I, L24S, del25-27, G142D, V213G, G339D, S371F,

843 S373P, S375F, T376A, D405N, R408S, K417N, N440K, G446S, S477N, T478K, E484A, Q493R,
844 Q498R, N501Y, Y505H, D614G, H655Y, N679K, P681H, N764K, D796Y, Q954H, N969K)

845 were assembled from three synthesized DNA fragments. The S6P expression construct containing
846 the Omicron BA.4/5 mutations (T19I, L24S, del25-27, del69-70, G142D, V213G, G339D, S371F,

847 S373P, S375F, T376A, D405N, R408S, K417N, N440K, G446S, L452R, S477N, T478K, E484A,
848 F486V, Q498R, N501Y, Y505H, D614G, H655Y, N658S, N679K, P681H, N764K, D796Y,

849 Q954H, N969K) were assembled from three synthesized DNA fragments. The expression
850 constructs encoding the SARS-CoV spike ectodomain (residues 1-1195)⁵⁰ was kindly provided by

851 Prof. X. Wang (Tsinghua University), and two stabilizing Pro substitutions (K968P, V969P) was
852 engineered into this construct using mutagenesis. For protein production, these expression

853 plasmids, as well as the plasmids encoding the antigen-binding fragments (Fabs) of the antibodies
854 described in this paper, were transfected into the HEK293F cells using polyethylenimine

855 (Polysciences). The conditioned media were harvested and concentrated using a Hydrosart

856 ultrafilter (Sartorius), and exchanged into the binding buffer (25 mM Tris, pH 8.0, and 200 mM
857 NaCl). Protein purifications were performed using the Ni-NTA affinity method, followed by gel
858 filtration chromatographies using either a Superose 6 increase column (for the spike proteins) or a
859 Superose 200 increase column (for the Fabs). The final buffer used for all proteins is 20 mM
860 HEPES, pH 7.2, and 150 mM NaCl.

861

862 **Cryo-EM data collection, processing, and structure building**

863 The samples for cryo-EM study were prepared essentially as previously described^{15,51}
864 (Supplementary Table 4). All EM grids were evacuated for 2 min and glow-discharged for 30 s
865 using a plasma cleaner (Harrick PDC-32G-2). Four microliters of spike protein (0.8 mg/mL) was
866 mixed with the same volume of Fabs (1 mg/mL each), and the mixture was immediately applied
867 to glow-discharged holy-carbon gold grids (Quantifoil, R1.2/1.3) in an FEI Vitrobot IV (4 °C and
868 100% humidity). Data collection was performed using either a Titan Krios G3 equipped with a K3
869 direct detection camera, or a Titan Krios G2 with a K2 camera, both operating at 300 kV. Data
870 processing was carried out using cryoSPARC (v3.2.1)⁵². After 2D classification, particles with
871 good qualities were selected for global 3D reconstruction and then subjected to homogeneous
872 refinement. To improve the density surrounding the RBD-Fab region, UCSF Chimera (v1.16)⁵³
873 and Relion (v3.1)⁵⁴ were used to generate the masks, and local refinement was then performed
874 using cryoSPARC (v3.2.1). Coot (v0.8.9.2)⁵⁵ and Phenix (v1.20)⁵⁶ were used for structural
875 modeling and refinement. Figures were prepared using UCSF ChimeraX (v1.3)⁵⁷ and Pymol
876 (v2.6.0a0, Schrödinger, LLC).

877

878 **Molecular dynamics simulation**

879 Models of the RBD from BA.1, BA.2, BA.3, BA.2.13, BA.2.12.1 and BA.4 in complex with ACE2
880 were firstly referred to the cryo-EM structure of BA.1-hACE2 (PDB code: 7WGB) and then
881 checked by WHAT IF Web Interface to remove atomic clashes. After that, the structures were
882 simulated by the software GROMACS-2021⁵⁸. Briefly, OPLS force field with TIP3P water model
883 was selected to prepare the dynamic system. After that Na⁺ and Cl⁻ ions were added into the system

884 to make the system electrically neutralized. Then, energy minimization using the steepest descent
885 algorithm was carried out until the maximum force of 1,000 kJ mol⁻¹ has been achieved. NVT
886 ensemble via the Nose-Hoover method at 300 K and NPT ensemble at 1 bar with the Parinello-
887 Rahman algorithm were employed successively to make the temperature and the pressure
888 equilibrated, respectively. Finally, MD production runs of 10 ns were performed with random
889 initial velocities and periodic boundary conditions. The non-bonded interactions were treated using
890 Verlet cut-off scheme, while the long-range electrostatic interactions were treated using particle
891 mesh Ewald (PME) method⁵⁸. The short-range electrostatic and van der Waals interactions were
892 calculated with a cut-off of 12 Å. All the 6 models were simulated in the same protocol.

893

894 **References**

895

- 896 42 Cao, Y. *et al.* Humoral immunogenicity and reactogenicity of CoronaVac or ZF2001 booster after two doses
897 of inactivated vaccine. *Cell Research* **32**, 107-109, doi:10.1038/s41422-021-00596-5 (2022).
- 898 43 Zheng, H. *et al.* Disease profile and plasma neutralizing activity of post-vaccination Omicron BA.1 infection
899 in Tianjin, China: a retrospective study. *Cell Research*, doi:10.1038/s41422-022-00674-2 (2022).
- 900 44 World Health Organization, *Living guidance for clinical management of COVID-19: living guidance* (2021).
- 901 45 Hao, Y. *et al.* Integrated analysis of multimodal single-cell data. *Cell* **184**, 3573-3587 e3529,
902 doi:10.1016/j.cell.2021.04.048 (2021).
- 903 46 Aran, D. *et al.* Reference-based analysis of lung single-cell sequencing reveals a transitional profibrotic
904 macrophage. *Nature Immunology* **20**, 163-172, doi:10.1038/s41590-018-0276-y (2019).
- 905 47 Monaco, G. *et al.* RNA-Seq Signatures Normalized by mRNA Abundance Allow Absolute Deconvolution of
906 Human Immune Cell Types. *Cell Reports* **26**, 1627-1640.e1627,
907 doi:<https://doi.org/10.1016/j.celrep.2019.01.041> (2019).
- 908 48 Ehrenmann, F. & Lefranc, M. P. IMGT/DomainGapAlign: IMGT standardized analysis of amino acid
909 sequences of variable, constant, and groove domains (IG, TR, MH, IgSF, MhSF). *Cold Spring Harb Protoc*
910 **2011**, 737-749, doi:10.1101/pdb.prot5636 (2011).
- 911 49 Starr, T. N. *et al.* Shifting mutational constraints in the SARS-CoV-2 receptor-binding domain during viral
912 evolution. *bioRxiv*, 2022.2002.2024.481899, doi:10.1101/2022.02.24.481899 (2022).
- 913 50 Gui, M. *et al.* Cryo-electron microscopy structures of the SARS-CoV spike glycoprotein reveal a prerequisite
914 conformational state for receptor binding. *Cell Res* **27**, 119-129, doi:10.1038/cr.2016.152 (2017).
- 915 51 Du, S. *et al.* Structures of SARS-CoV-2 B.1.351 neutralizing antibodies provide insights into cocktail design
916 against concerning variants. *Cell Res* **31**, 1130-1133, doi:10.1038/s41422-021-00555-0 (2021).
- 917 52 Punjani, A., Rubinstein, J. L., Fleet, D. J. & Brubaker, M. A. cryoSPARC: algorithms for rapid unsupervised
918 cryo-EM structure determination. *Nat Methods* **14**, 290-296, doi:10.1038/nmeth.4169 (2017).
- 919 53 Pettersen, E. F. *et al.* UCSF Chimera--a visualization system for exploratory research and analysis. *J Comput*
920 *Chem* **25**, 1605-1612, doi:10.1002/jcc.20084 (2004).

- 921 54 Zivanov, J. *et al.* New tools for automated high-resolution cryo-EM structure determination in RELION-3.
922 *Elife* **7**, doi:10.7554/eLife.42166 (2018).
- 923 55 Emsley, P., Lohkamp, B., Scott, W. G. & Cowtan, K. Features and development of Coot. *Acta*
924 *crystallographica. Section D, Biological crystallography* **66**, 486-501, doi:10.1107/S0907444910007493
925 (2010).
- 926 56 Liebschner, D. *et al.* Macromolecular structure determination using X-rays, neutrons and electrons: recent
927 developments in Phenix. *Acta Crystallogr D Struct Biol* **75**, 861-877, doi:10.1107/S2059798319011471
928 (2019).
- 929 57 Pettersen, E. F. *et al.* UCSF ChimeraX: Structure visualization for researchers, educators, and developers.
930 *Protein Sci* **30**, 70-82, doi:10.1002/pro.3943 (2021).
- 931 58 Abraham, M. J. *et al.* GROMACS: High performance molecular simulations through multi-level parallelism
932 from laptops to supercomputers. *SoftwareX* **1-2**, 19-25, doi:<https://doi.org/10.1016/j.softx.2015.06.001>
933 (2015).

934

935 **Data availability**

936 Processed mutation escape scores can be downloaded at [https://github.com/jianfcpk/SARS-CoV-](https://github.com/jianfcpk/SARS-CoV-2-RBD-DMS-broad)
937 [2-RBD-DMS-broad](https://github.com/jianfcpk/SARS-CoV-2-RBD-DMS-broad). Raw Illumina and PacBio sequencing data are available on NCBI Sequence
938 Read Archive BioProject PRJNA804413. We used vdj_GRCh38_alts_ensembl-5.0.0 as the
939 reference of V(D)J alignment, which can be obtained from

940 <https://support.10xgenomics.com/single-cell-vdj/software/downloads/latest>.

941 IMGT/DomainGapAlign is based on the built-in latest IMGT antibody database, and we let the
942 “Species” parameter as “Homo sapiens” while kept the others as default. Public deep mutational
943 scanning datasets involved in the study from literature could be downloaded at
944 [https://media.githubusercontent.com/media/jbloomb/SARS2_RBD_Ab_escape_maps/main/pro-](https://media.githubusercontent.com/media/jbloomb/SARS2_RBD_Ab_escape_maps/main/processed_data/escape_data.csv)
945 [cessed_data/escape_data.csv](https://media.githubusercontent.com/media/jbloomb/SARS2_RBD_Ab_escape_maps/main/processed_data/escape_data.csv).

946 Public structures involved in this manuscript were downloaded from Protein Data Bank with
947 accession codes 6M0J, 7K8V, 7MMO, 7EY0, 7DX4, 7M7W, 7JW0, 7WPB, 7WGB.

948 Cryo-EM density maps have been deposited in the Electron Microscopy Data Bank with accession
949 codes EMD-33210, EMD-33211, EMD-33212, EMD-33213, EMD-33323, EMD-33324, EMD-
950 33325, EMD-32732, EMD-32738, EMD-32734, EMD-32718, and EMD-33019, respectively.

951 Structural coordinates have been deposited in the Protein Data Bank with accession codes 7XIW,
952 7XIX, 7XIY, 7XIZ, 7XNQ, 7XNR, 7XNS 7WRL, 7WRZ, 7WRO, 7WR8 and 7X6A.

953

954 **Code availability**

955 Python and R scripts for analyzing escaping mutation profile data and reproducing figures in this
956 manuscript are available at <https://github.com/jianfcpk/SARS-CoV-2-RBD-DMS-broad>.

957

958 **Ethical Statement**

959 This study was approved by the Ethics Committee of Beijing Ditan Hospital affiliated to Capital
960 Medical University (Ethics committee archiving No. LL-2021-024-02), the Tianjin Municipal
961 Health Commission, and the Ethics Committee of Tianjin First Central Hospital (Ethics committee
962 archiving No. 2022N045KY). Informed consent was obtained from all human research
963 participants.

964

965 **Acknowledgments**

966 We thank J. Bloom for his gift of the yeast SARS-CoV-2 WT RBD libraries. We thank Sino
967 Biological for the technical assistance on mAbs and RBD expression. We thank J. Luo and H. Lv
968 for the help with flow cytometry. This project is financially supported by the Ministry of Science
969 and Technology of China (CPL-1233).

970

971 **Author contributions**

972 Y.Cao and X.S.X designed the study. Y.Cao, F.J. and X.S.X wrote the manuscript with inputs
973 from all authors. Y.Cao. and F.S. coordinated the expression and characterization of the
974 neutralizing antibodies. J.W. (BIOPIC), F.J., L.Z., H.S. performed and analyzed the yeast display
975 screening experiments. Y.Y., T.X., P.W., J.W. (Changping Laboratory), R.A., Y.W., J.Z., N.Z.,
976 R.W., X.N., L.Y., C.L., X.S. L.Z., F.S. performed the neutralizing antibody expression and
977 characterization, including pseudovirus neutralization and ELISA. Y.Y., W.H., Q.L., Y.W.
978 prepared the VSV-based SARS-CoV-2 pseudovirus. A.Y., Y.W., S.Y., R.A., W.S. performed and
979 analyzed the antigen-specific single B cell VDJ sequencing. S.D., P.L., Z.Z., L.W., R.F., Z.L.,
980 X.W., J.X. performed the structural analyses. X.H., W.Z., D.Z., and R.J. recruited the SARS

981 convalescents and SARS-CoV-2 vaccinees. X.C. and Z.S. recruited the Omicron BA.1
982 convalescents. X.C., Y.Chai, Y.H., and Y.S. isolated PBMC from BA.1 convalescents. Q.G.
983 proofed the manuscript.

984

985 **Competing interests**

986 X.S.X. and Y.C. are inventors on the provisional patent applications of BD series antibodies, which
987 includes BD30-604 (DXP-604), BD55-5840 (SA58) and BD55-5514 (SA55). X.S.X. and Y.C. are
988 founders of Singlomics Biopharmaceuticals. Other authors declare no competing interests.

989

990 **Extended Data Figures**

991

992 **Extended Data Fig. 1 | Structures and ACE2 binding of emerging Omicron subvariants spike 993 glycoprotein.**

994 **a**, Mutations on the spike glycoprotein of SARS-CoV-2 Omicron subvariants. Residues that are
995 not identical among Omicron subvariants are colored red. **b**, Workflow to generate cryo-EM
996 structure of BA.2, BA.3, BA.2.13, BA.2.12.1, BA.4/5 spike glycoprotein trimer with S6P and
997 R683A, R685A substitutions. **c**, Binding affinities of Omicron variants spike trimers to hACE2
998 measured by SPR. SPR analyses were conducted in biological duplicates. **d**, MD simulated
999 interactions between hACE2 and RBD of Omicron variants. Structures of the RBD from Omicron
1000 variants and hACE2 are shown as ribbons.

1001

1002 **Extended Data Fig. 2 | Different immunity backgrounds lead to distinct humoral immunity 1003 against Omicron subvariants**

1004 NT50 against SARS-CoV-2, SARS-CoV-1 D614G and Omicron subvariants spike-pseudotyped
1005 VSV by plasma samples from **a**, individuals who received 3 doses CoronaVac with (n=50) or
1006 without (n=40) BA.1 breakthrough infection; **b**, individuals who received 2 doses CoronaVac and
1007 ZF2001 booster with (n=28) or without (n=38) previous SARS-CoV-1 infection; **c**, individuals
1008 who received 3 doses CoronaVac (n=40) or 2 doses CoronaVac with ZF2001 booster (n=38). P-
1009 values were calculated using two-tailed Wilcoxon rank-sum tests and labeled above the bars. n.s.,
1010 not significant, $p > 0.05$. All neutralization assays were conducted in biological duplicates.
1011 Geometric means are labeled. Error bars refer to geometric standard deviations.

1012

1013 **Extended Data Fig. 3 | Workflow for the isolation and characterization of SARS-CoV-2 RBD 1014 antibodies.**

1015 **a**, Overall schematic of antibody identification by single cell VDJ sequencing with feature
1016 barcodes and epitope analysis by high-throughput deep mutational scanning. **b**, FACS strategy to
1017 enrich BA.1/WT cross-reactive memory B cells or BA.1-specific memory B cells.

1018

1019 **Extended Data Fig. 4 | ELISA reactivity against 22 sarbecovirus RBD.**

1020 Shades of red indicate ELISA OD450 for each antibody against various sarbecoviruses from
1021 different clades.

1022

1023 **Extended Data Fig. 5 | Neutralizing activities of antibodies elicited by SARS-CoV-2 BA.1 or
1024 wildtype.**

1025 Neutralizing activity against SARS-CoV-2 D614G and Omicron subvariants pseudovirus by
1026 antibodies of each epitope group from BA.1 convalescents (BA.1-stimulated. A, n=30; B, n=41;
1027 C, n=20; D1, n=49; D2, n=17; E1, n=11; E2.1, n=64; E2.2, n=122; E3, n=57; F1, n=80; F2, n=13;
1028 F3, n=2), and from wildtype convalescents or vaccinees (WT-stimulated. A, n=98; B, n=55; C,
1029 n=88; D1, n=46; D2, n=36; E1, n=59; E2.1, n=26; E2.2, n=39; E3, n=68; F1, n=97; F2, n=158;
1030 F3, n=67). Geometric mean titers (GMT) are annotated above each group of points, and error bars
1031 indicate geometric standard deviation. P-values were calculated using two-tailed Wilcoxon rank-
1032 sum tests and labeled above the bars. n.s., not significant, $p>0.05$. NAbs in the boxed epitope
1033 groups showed substantial neutralization potency changes against BA.2.12.1 or BA.4/5 compared
1034 to BA.1. All neutralization assays were conducted in biological duplicates.

1035

1036 **Extended Data Fig. 6 | Heavy chain V-J genes of BA.1-stimulated and WT-stimulated
1037 antibodies in each epitope group.**

1038 Heavy chain V-J genes combination of **a**, WT-stimulated antibodies. **b**, BA.1-stimulated antibodies
1039 or each epitope group. The number of NAbs is annotated above the chord plot. IGHV genes are
1040 annotated only if the corresponding number of antibodies is greater than one.

1041

1042 **Extended Data Fig. 7 | Comparison of BA.1-stimulated and WT-stimulated antibodies in
1043 group A, B and C.**

1044 **a**, Neutralizing activity against SARS-CoV-2 D614G and Omicron subvariants by BA.1-
1045 stimulated (A, n=30; B, n=41; C, n=20) and WT-stimulated (A, n=98; B, n=55; C, n=88) antibodies
1046 in Group A, B and C. Geometric mean of IC50 fold changes compared to IC50 against BA.2 are
1047 annotated above the bars. P-values were calculated using a two-tailed Wilcoxon signed-rank test
1048 of paired samples, in comparison to IC50 against BA.2. *, $p<0.05$; **, $p<0.01$; ***, $p<0.001$; n.s.,
1049 not significant, $p>0.05$. All neutralization assays were conducted in biological duplicates. **b**,
1050 Averaged escape maps at escape hotspots of BA.1-stimulated and WT-stimulated antibodies in
1051 group A, B and C, and corresponding MSA of various sarbecovirus RBDs. Height of each amino
1052 acid in the escape maps represents its mutation escape score. Mutated sites in Omicron variants
1053 are marked in bold.

1054

1055 **Extended Data Fig. 8 | Antibodies of group E3 and F1 exhibit weak but broad-spectrum
1056 neutralization.**

1057 **a**, Neutralizing activity against SARS-CoV-2 D614G and Omicron subvariants by antibodies in
1058 group E3 (n=125) and F1 (n=177). Geometric mean of IC50 fold changes compared to BA.2 are
1059 annotated above the bars. P-values were calculated using a two-tailed Wilcoxon signed-rank test

1060 of paired samples, in comparison to IC50 against BA.2. *, $p < 0.05$; **, $p < 0.01$; ***, $p < 0.001$; n.s.,
1061 not significant, $p > 0.05$. All neutralization assays were conducted in biological duplicates. **b**,
1062 Epitope of representative antibodies in group E3 (S2H97, PDB: 7M7W) and F1 (S304, PDB:
1063 7JW0). Residues highlighted in red indicate mutated sites in Omicron variants. **c**, Averaged escape
1064 maps at escape hotspots of antibodies in group E3 and F1, and corresponding MSA of various
1065 sarbecovirus RBDs. Height of each amino acid in the escape maps represents its mutation escape
1066 score. Mutated sites in Omicron variants are marked in bold.

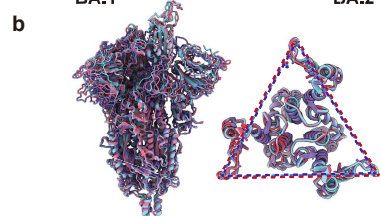
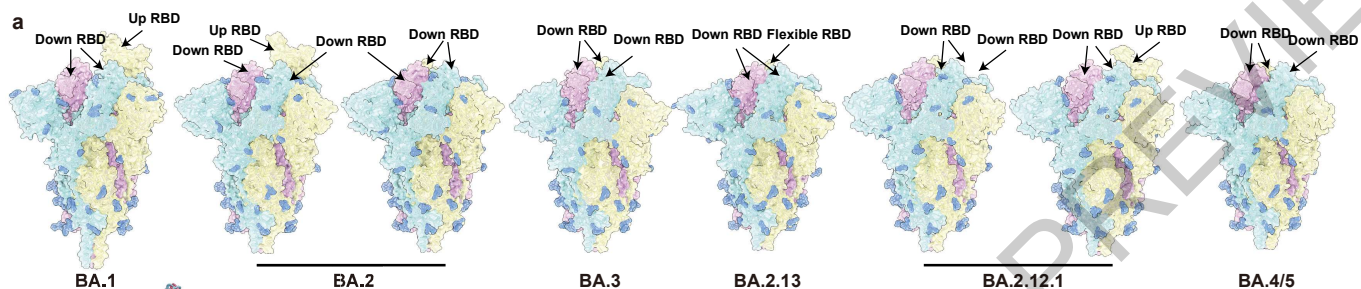
1067
1068 **Extended Data Fig. 9 | RBD-binding structures and affinity of broad Sarbecovirus antibodies.**

1069 **a**, Cartoon models of Cryo-EM structures of BD55-3152 in complex of BA.1 RBD, BD55-1239
1070 in complex of BA.1 RBD, and BD55-3372 in complex of Delta RBD. **b**, Workflow to generate
1071 refined structural model of BD55-3152 and BD55-1239 in complex of BA.1 RBD, BD55-3372 in
1072 complex of Delta RBD, and BD55-5840 in complex of BA.2 RBD. **c**, Neutralizing activity of
1073 representative NAbs in group E1 ($n=68$), F2 ($n=139$) and F3 ($n=61$) against SARS-CoV-2 D614G,
1074 in addition to D614G+D405N and D614G+R408S. Geometric mean of IC50 fold changes
1075 compared to IC50 against D614G are annotated above the bars. P-values were calculated using a
1076 two-tailed Wilcoxon signed-rank test of paired samples. *, $p < 0.05$; **, $p < 0.01$; ***, $p < 0.001$; n.s.,
1077 not significant, $p > 0.05$. All neutralization assays were conducted in biological duplicates. **d**,
1078 Conformational comparison between BA.1 and BA.2 RBD regarding the 366-377 hairpin. **e**,
1079 Biolayer interferometry analysis of Group E1 antibodies S309 and BD55-5840 binding to Omicron
1080 BA.1 and BA.2 Spike trimer. Biolayer interferometry analyses were conducted in biological
1081 duplicates.

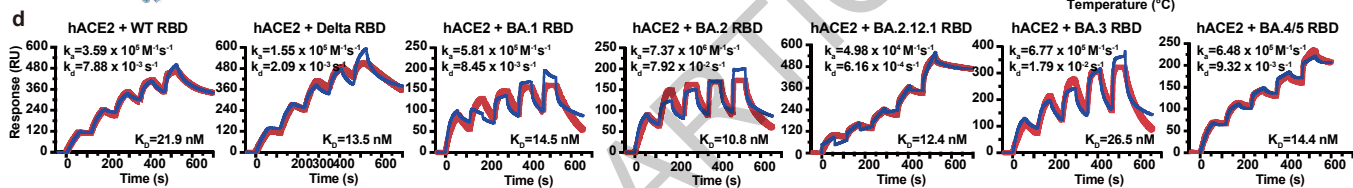
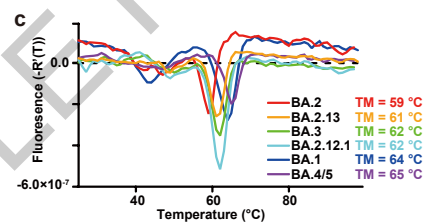
1082
1083 **Extended Data Fig. 10 | HV-HJ gene combination of BA.1-specific antibodies.**

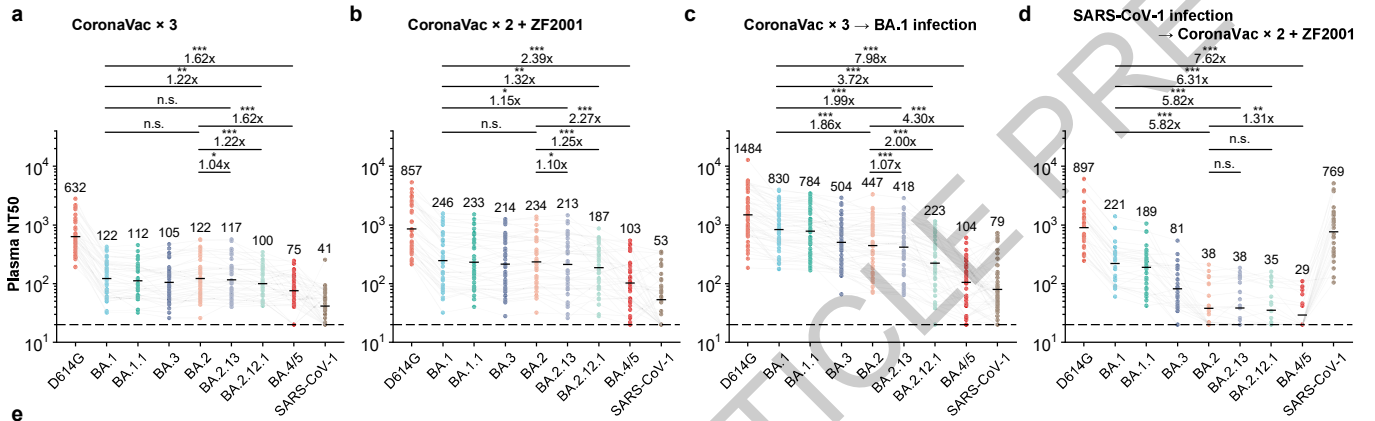
1084 Heavy chain V-J gene combination of BA.1-specific neutralizing antibodies in BA.1-specific
1085 epitope groups A^{Omi}, B^{Omi}, D^{Omi} and F3^{Omi}.

1086

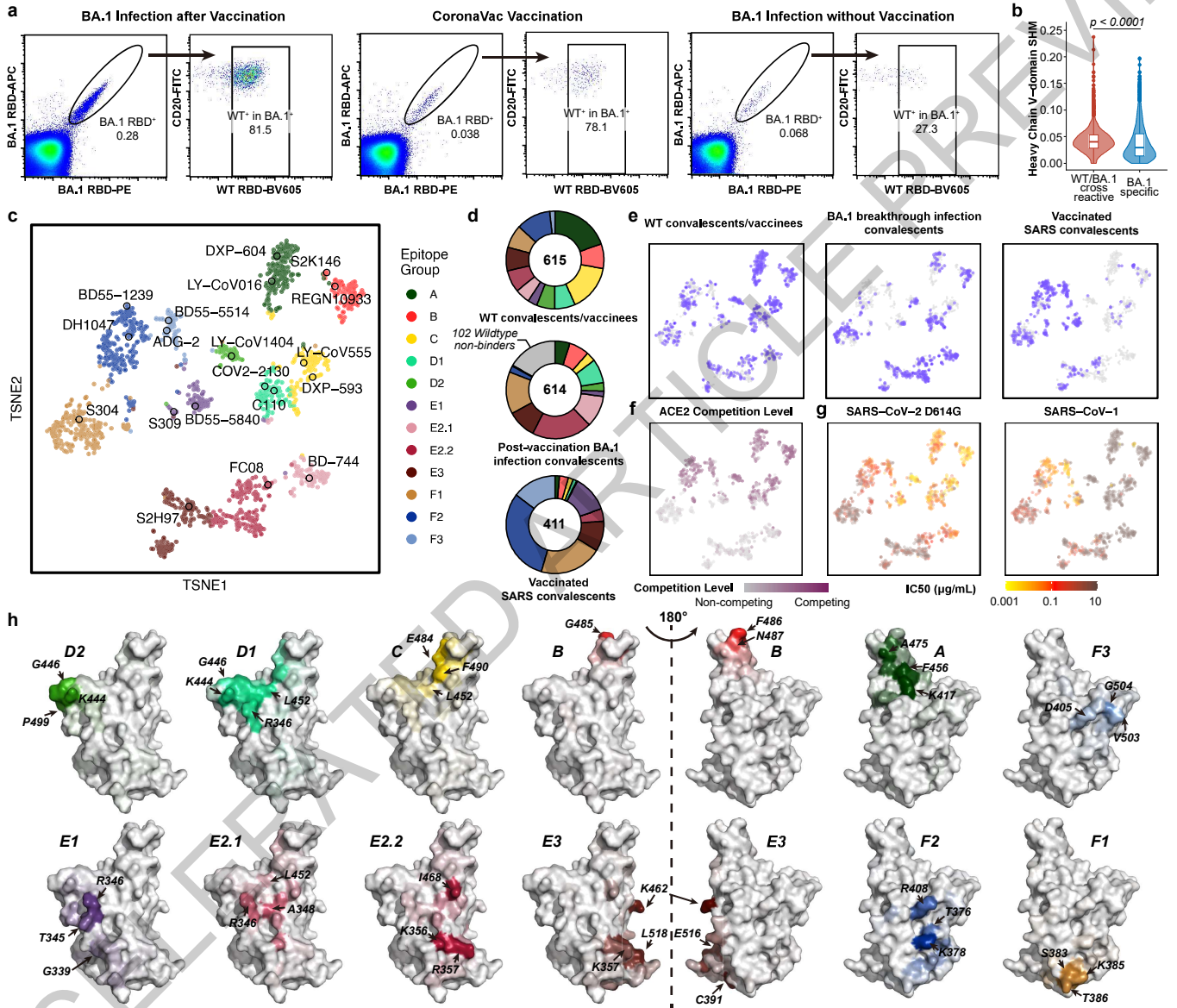


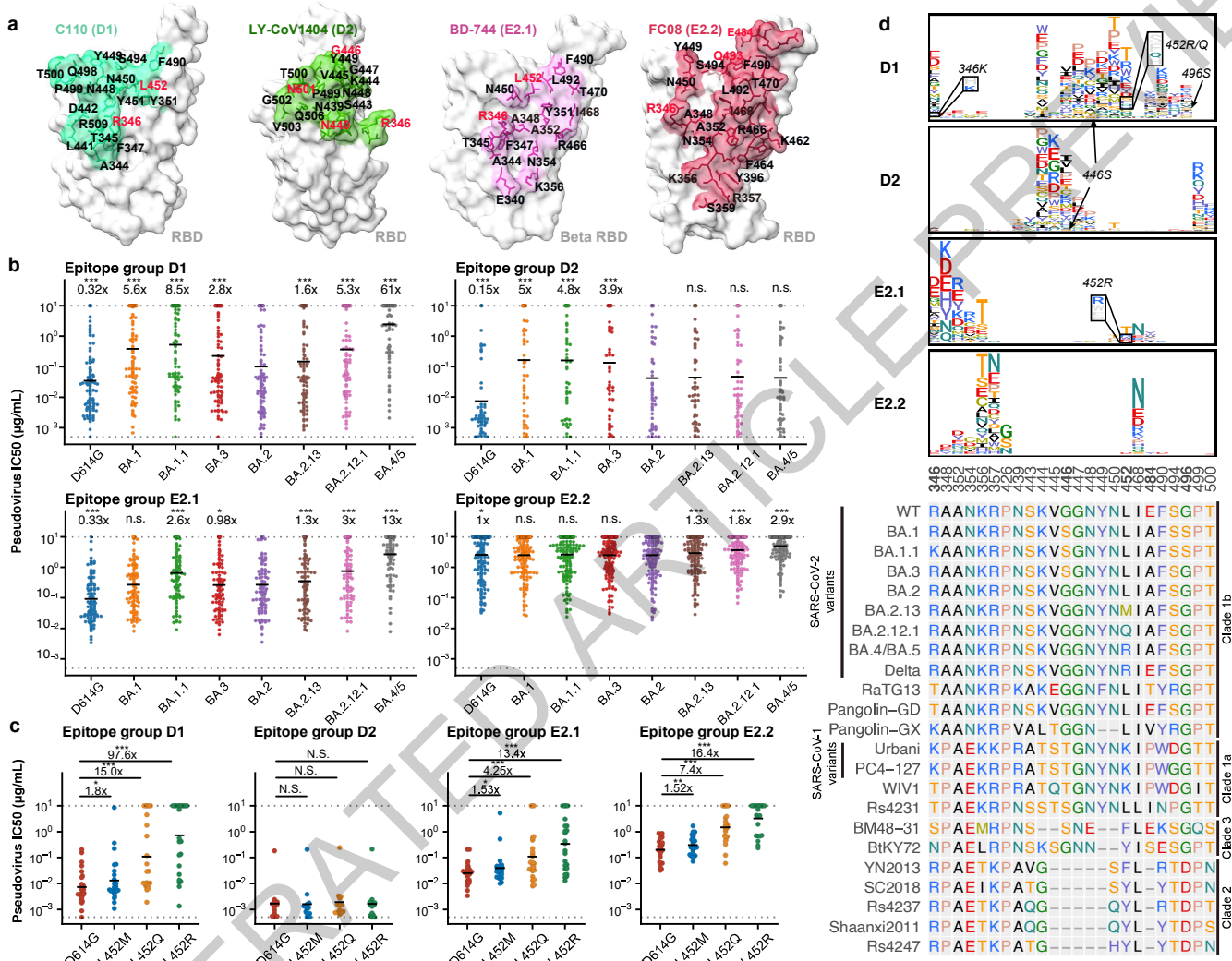
	AB (Å ²)	AC (Å ²)	BC (Å ²)	AVE. (Å ²)
BA.1	2,753.7	2,763.6	2,844.5	2,787.3
BA.2	2,650.9	2,642.4	2,583.1	2,625.5
BA.3	2,736.7	2,701.0	2,868.3	2,768.7
BA.2.13	2,495.5	2,517.6	2,525.1	2,512.7
BA.2.12.1	2,539.2	2,541.4	2,516.2	2,532.2
BA.4/5	2,801.0	2,806.7	2,808.9	2,805.5



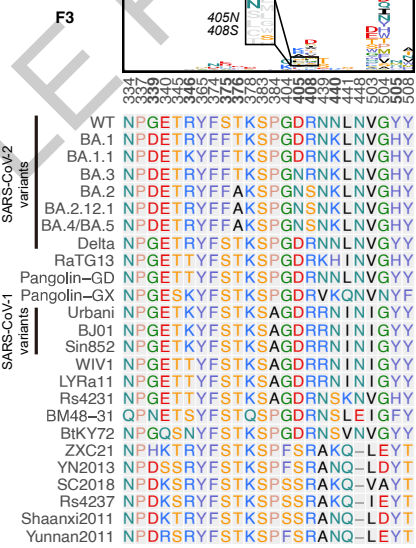
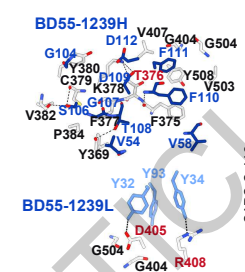
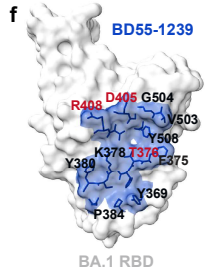
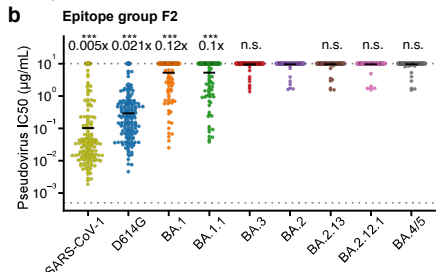
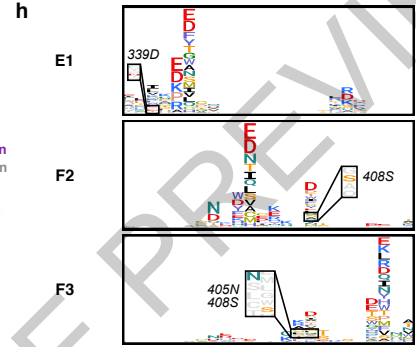
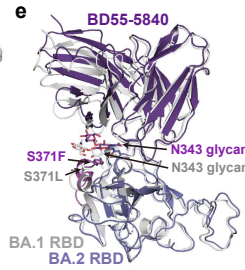
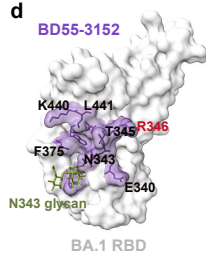
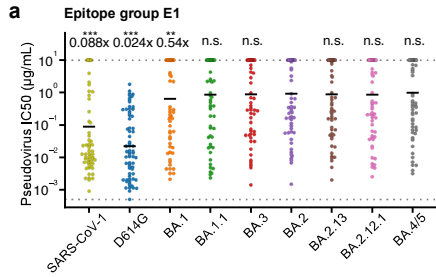


IC50 (ng/mL)	LY-CoV016	LY-CoV555	LY-CoV1404	REGN10933	REGN10987	COV2-2196	COV2-2130	BRIL-196	BRIL-198	S309	DXP-604	ADG-2	S2K146	SA58 (BD55-5840)	SA55 (BD55-5514)	LY-CoV016+	REGN10933+	COV2-2196+	BRIL-196+	SA55+SA58
D614G	32	15	0.7	5.6	5.7	1.6	2.5	53	1239	74	11	11	17	0.9	11	20	5.0	2.1	81	2.1
BA.1	*	*	0.6	*	*	5419	3007	7118	1171	361	285	979	11	4.4	1.7	*	*	491	1890	3.2
BA.1.1	*	*	1.8	8912	*	4764	*	6324	*	314	198	991	17	4.5	3.0	*	*	8090	*	3.3
BA.2	*	*	0.9	*	590	4312	6.3	8530	8990	918	219	*	20	12	7.2	*	821	8.2	8610	7.8
BA.3	*	*	1.1	*	*	5609	11	7833	1687	972	259	6226	16	8.1	7.1	*	*	19	2190	6.4
BA.2.13	*	*	1.0	9221	417	3591	6.6	6902	*	700	148	*	16	4.9	5.9	*	699	7.1	*	4.8
BA.2.12.1	*	*	0.8	*	499	5521	11	7620	*	989	201	*	13	5.0	5.2	*	714	18	*	5.0
BA.4/BA.5	*	*	0.9	*	520	*	23	7124	*	792	6264	*	221	3.9	5.0	*	709	40	*	4.5
SARS-CoV-1	*	*	*	*	*	*	*	*	*	31	*	1.7	108	5.6	4.4	*	*	*	*	4.6
Pangolin-GD	1125	6.8	8.6	157	84	17	*	13	*	7.4	5.0	14	296	5.7	10	98	27	33	7.7	
RaTG13	*	*	*	*	*	*	*	16	*	1.1	*	3.9	*	*	38	*	*	*	29	49

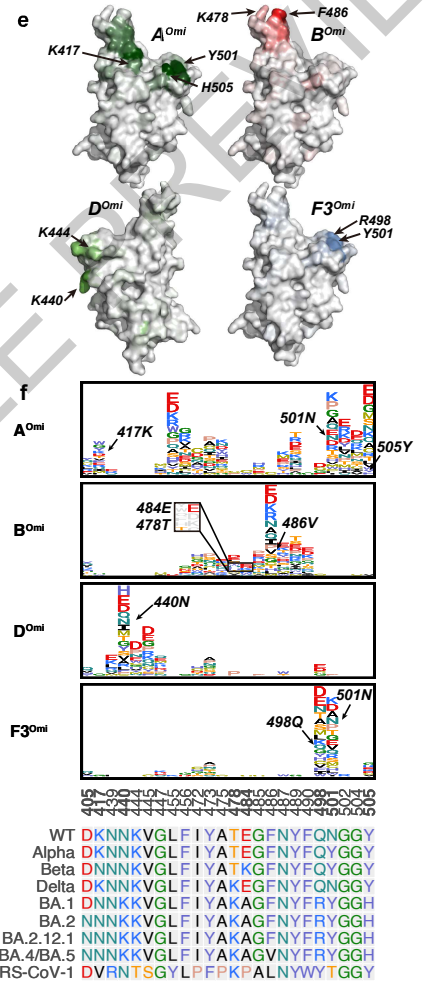
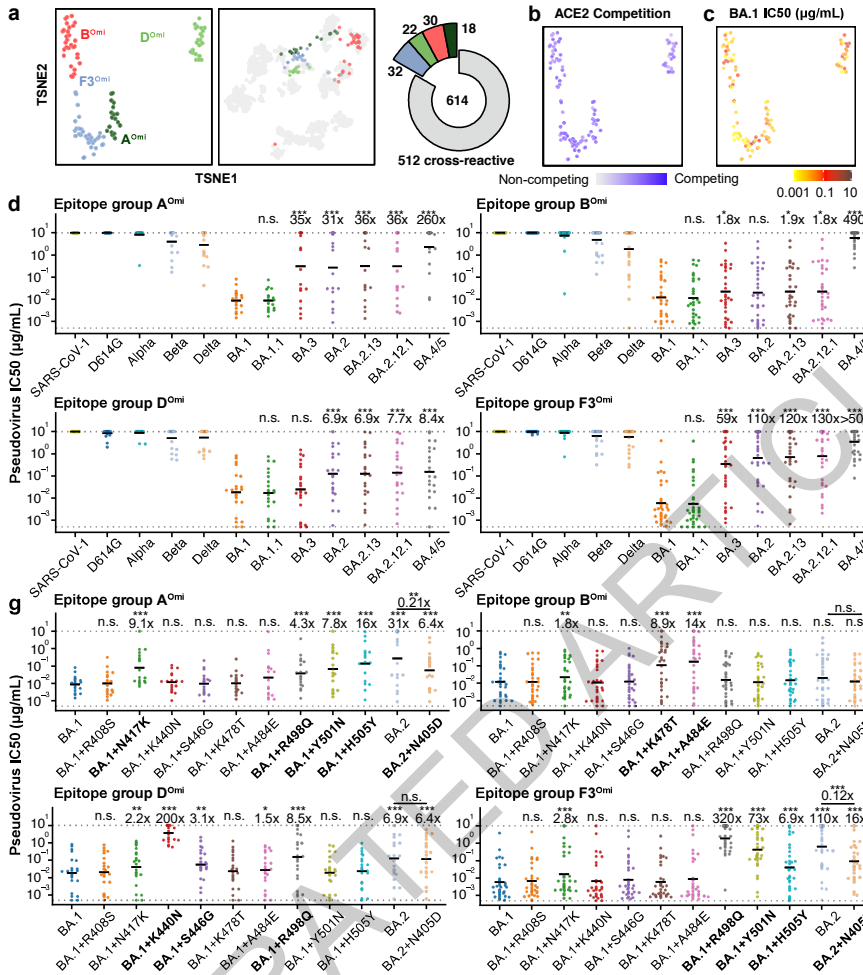


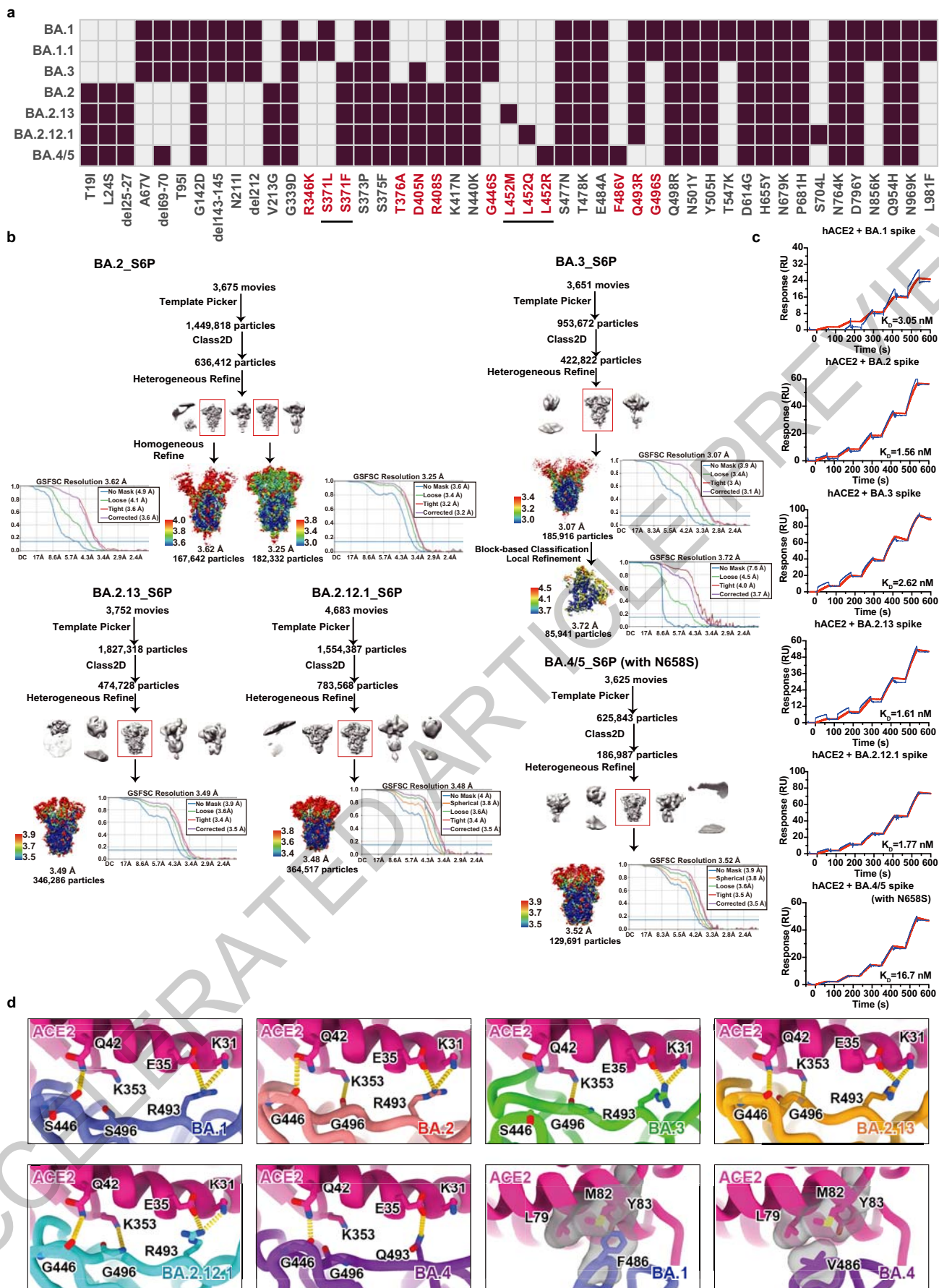


ACCELERATE YOUR RESEARCH

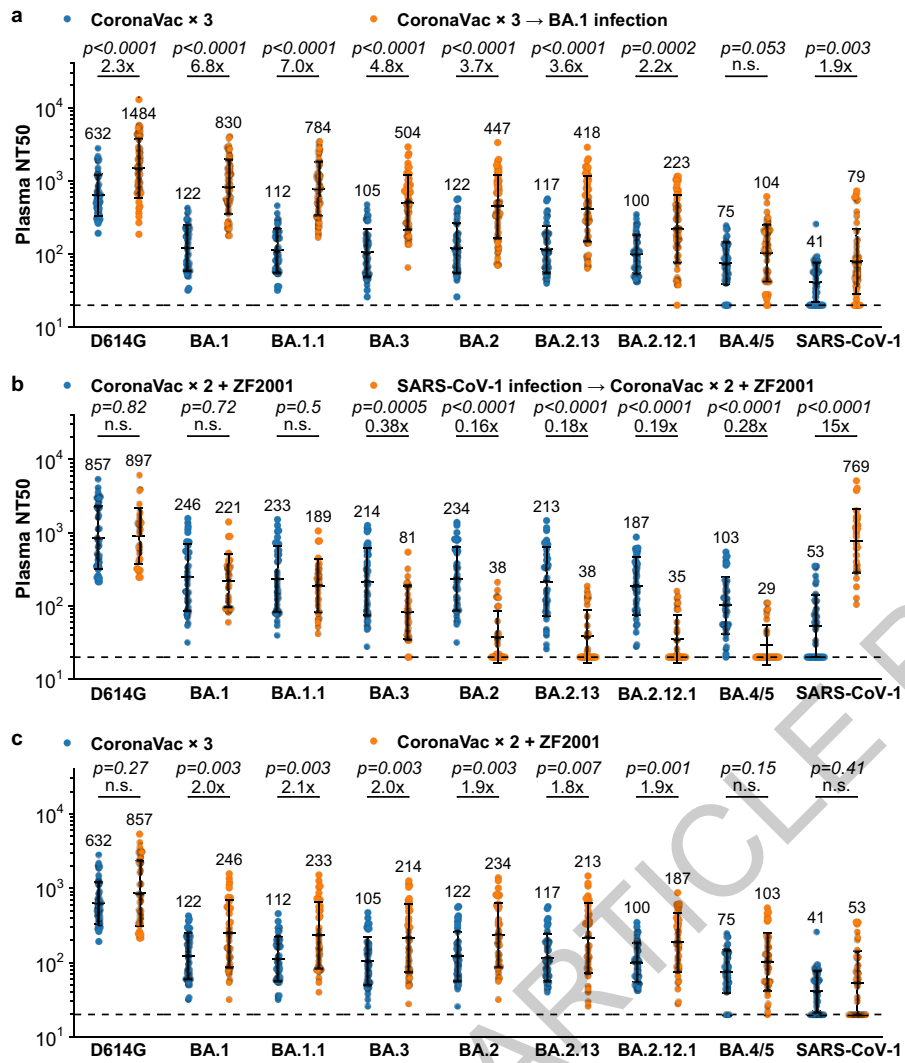


ACCELERATED PUBLICATION

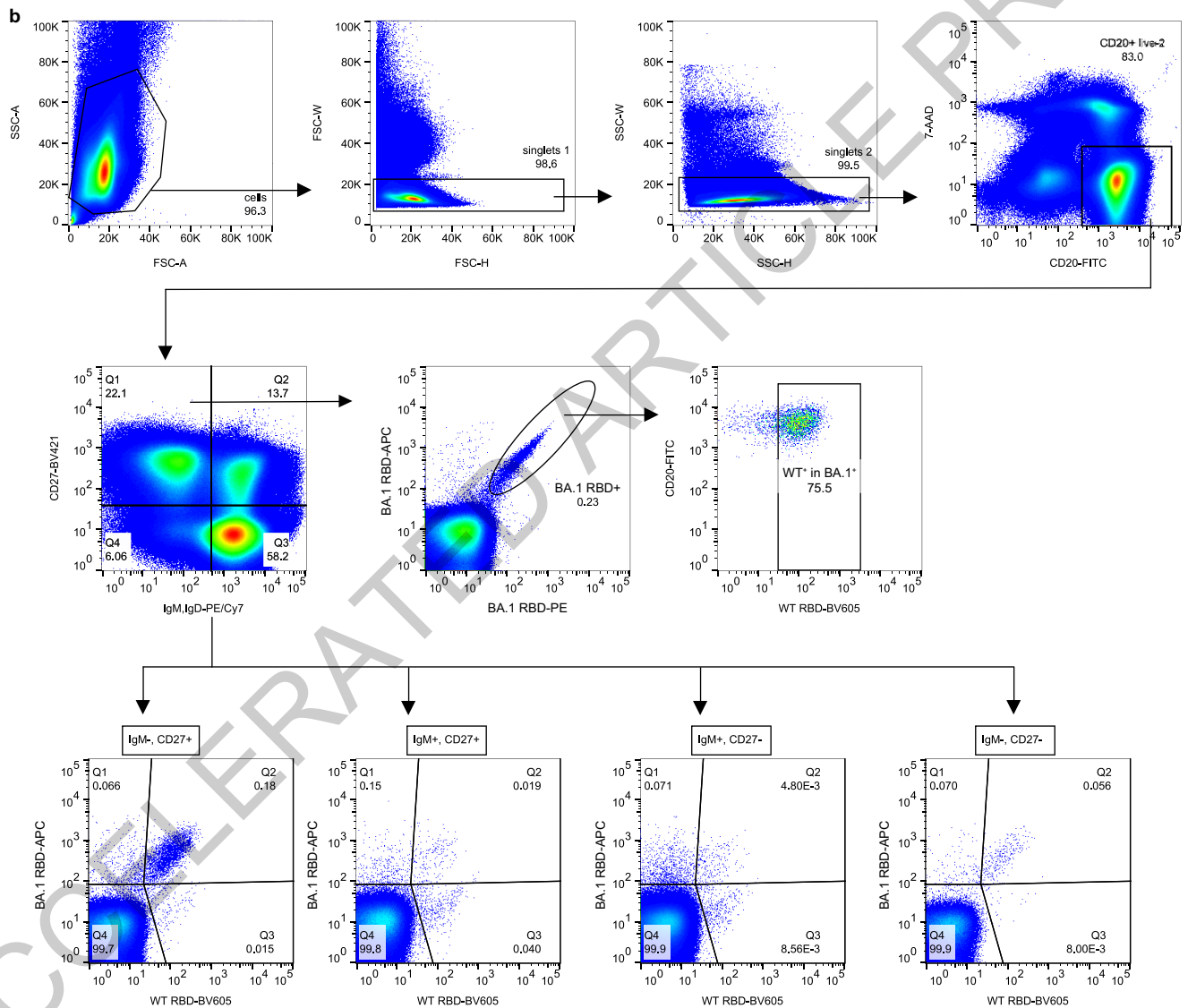
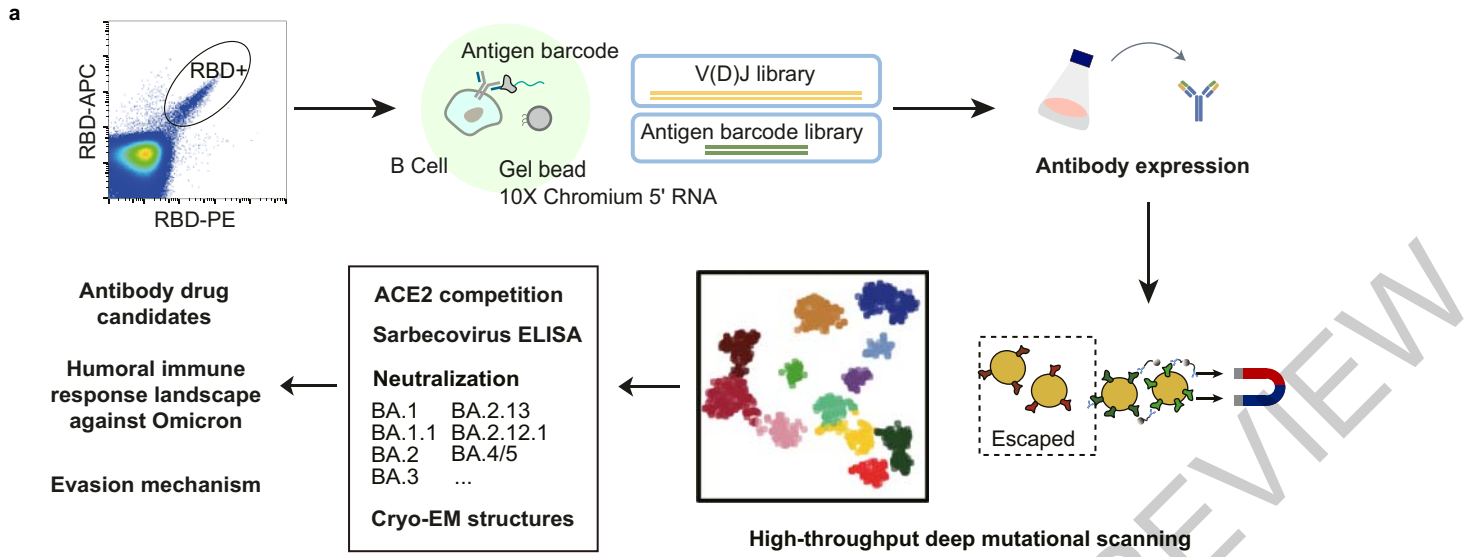




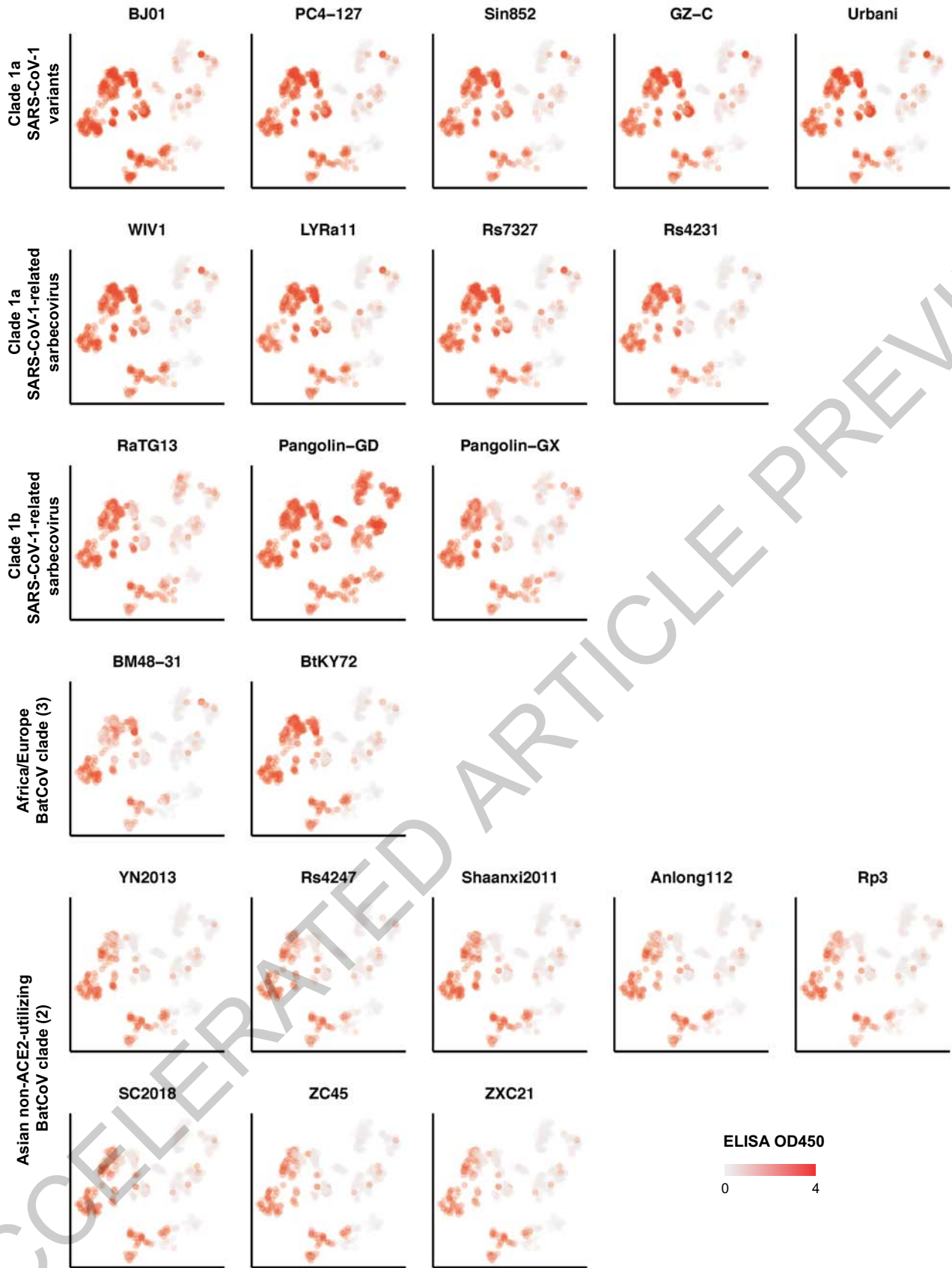
Extended Data Fig. 1



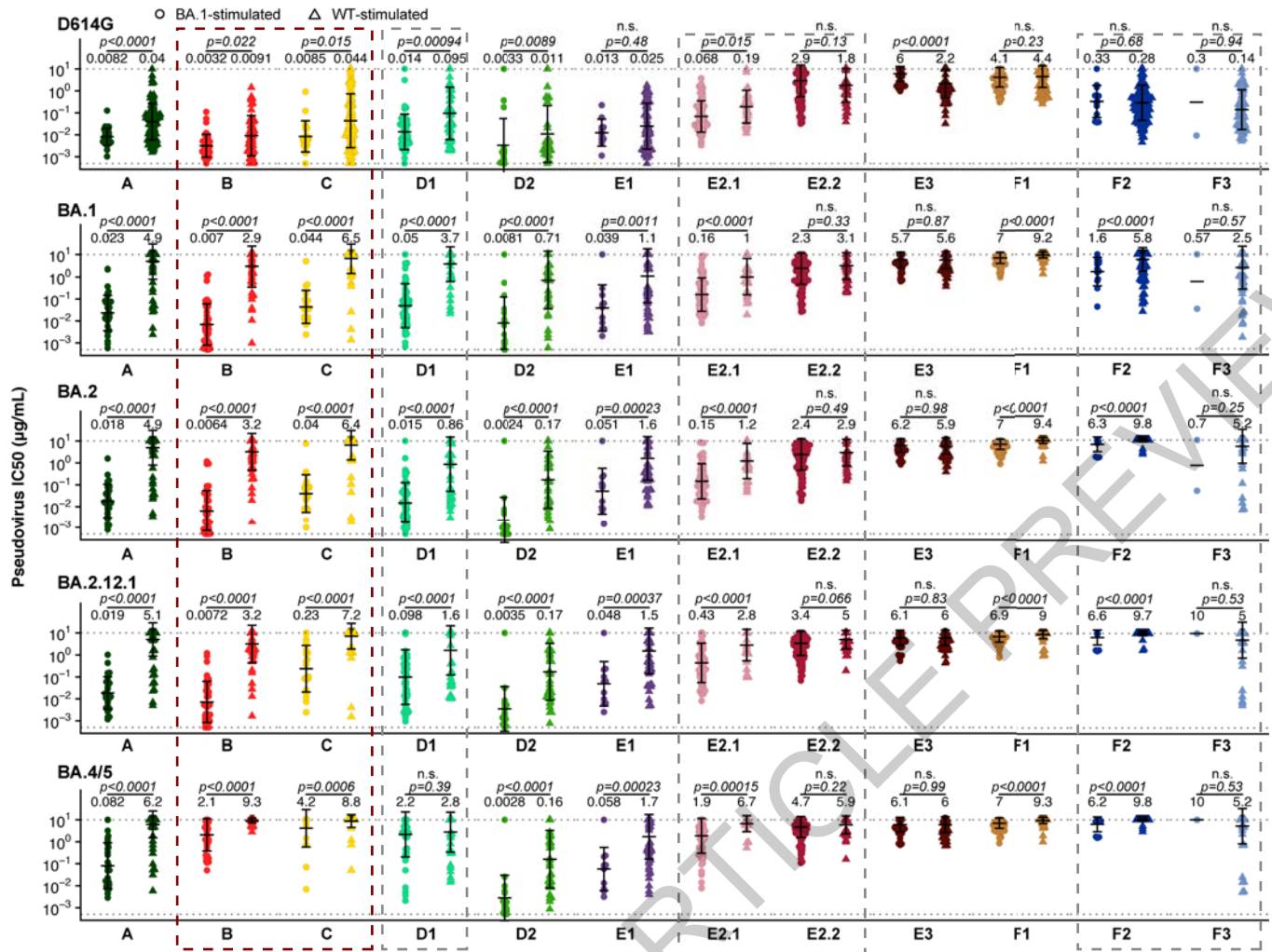
Extended Data Fig. 2



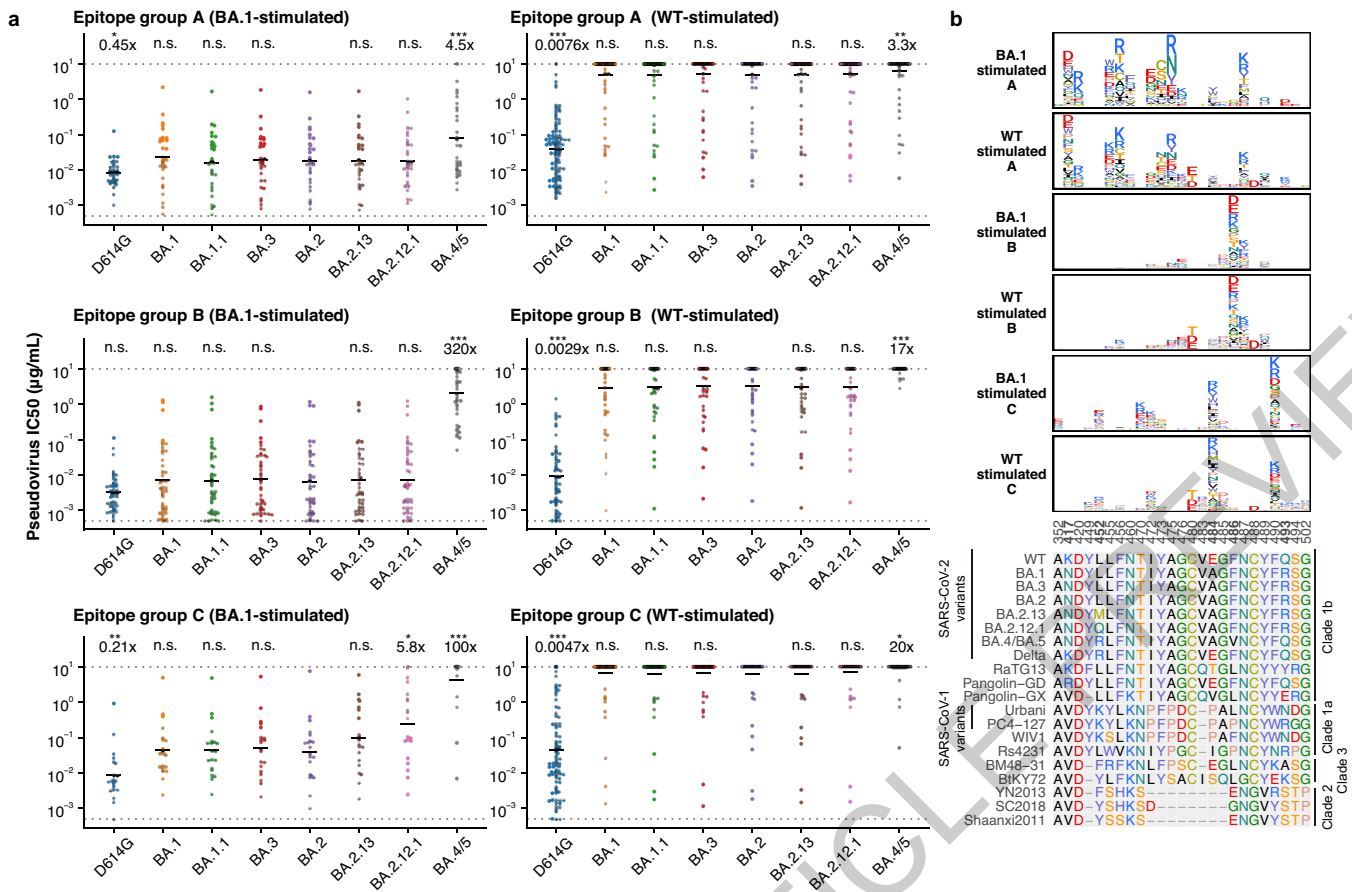
Extended Data Fig. 3



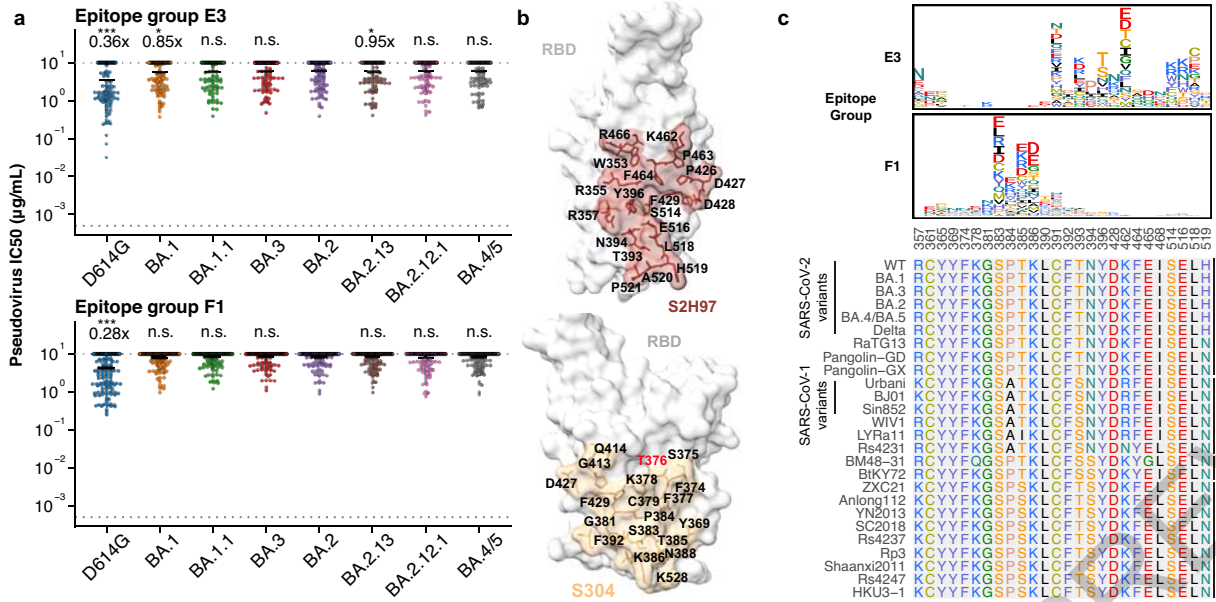
Extended Data Fig. 4



Extended Data Fig. 5

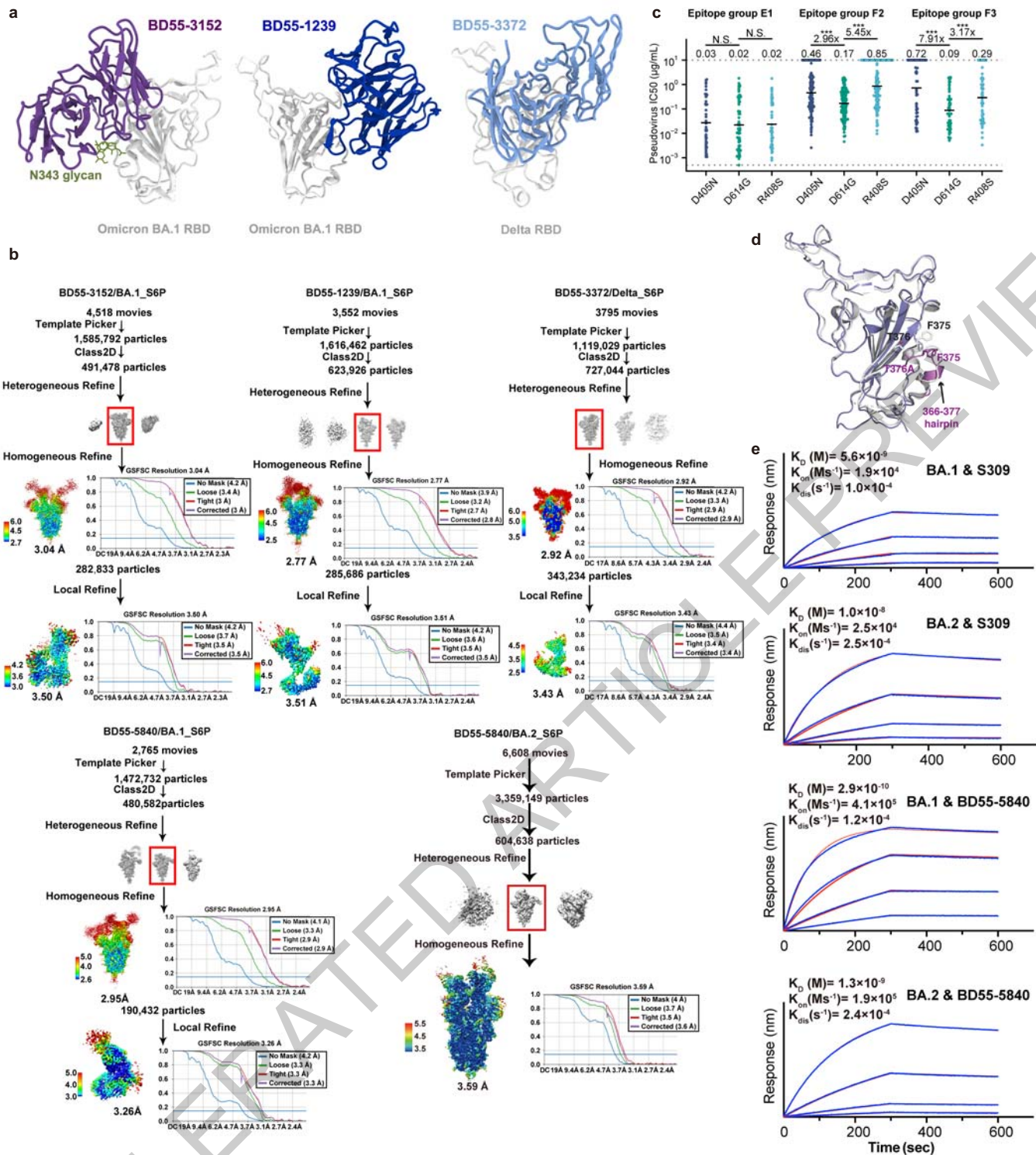


Extended Data Fig. 7

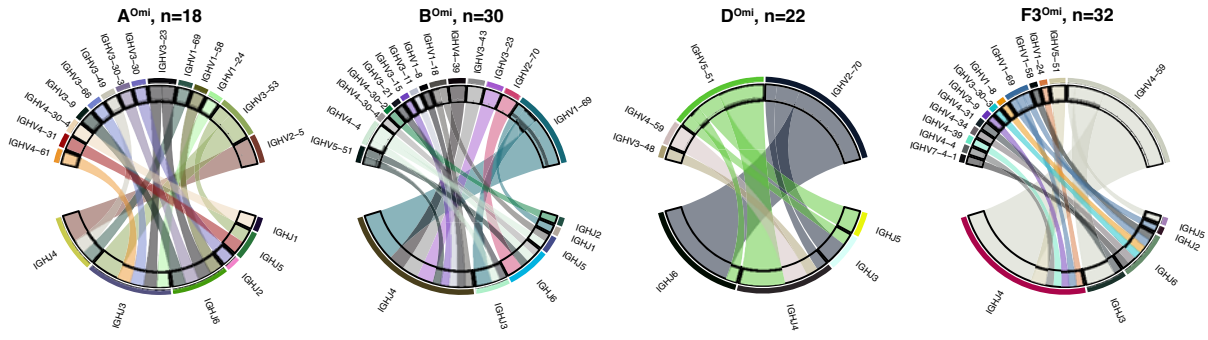


Extended Data Fig. 8

ACCELERATED ARTICLE PREVIEW



Extended Data Fig. 9



Extended Data Fig. 10

ACCELERATED ARTICLE PREVIEW

Reporting Summary

Nature Portfolio wishes to improve the reproducibility of the work that we publish. This form provides structure for consistency and transparency in reporting. For further information on Nature Portfolio policies, see our [Editorial Policies](#) and the [Editorial Policy Checklist](#).

Statistics

For all statistical analyses, confirm that the following items are present in the figure legend, table legend, main text, or Methods section.

- | n/a | Confirmed |
|-------------------------------------|--|
| <input type="checkbox"/> | <input checked="" type="checkbox"/> The exact sample size (n) for each experimental group/condition, given as a discrete number and unit of measurement |
| <input type="checkbox"/> | <input checked="" type="checkbox"/> A statement on whether measurements were taken from distinct samples or whether the same sample was measured repeatedly |
| <input type="checkbox"/> | <input checked="" type="checkbox"/> The statistical test(s) used AND whether they are one- or two-sided
<i>Only common tests should be described solely by name; describe more complex techniques in the Methods section.</i> |
| <input checked="" type="checkbox"/> | <input type="checkbox"/> A description of all covariates tested |
| <input checked="" type="checkbox"/> | <input type="checkbox"/> A description of any assumptions or corrections, such as tests of normality and adjustment for multiple comparisons |
| <input type="checkbox"/> | <input checked="" type="checkbox"/> A full description of the statistical parameters including central tendency (e.g. means) or other basic estimates (e.g. regression coefficient) AND variation (e.g. standard deviation) or associated estimates of uncertainty (e.g. confidence intervals) |
| <input type="checkbox"/> | <input checked="" type="checkbox"/> For null hypothesis testing, the test statistic (e.g. F , t , r) with confidence intervals, effect sizes, degrees of freedom and P value noted
<i>Give P values as exact values whenever suitable.</i> |
| <input checked="" type="checkbox"/> | <input type="checkbox"/> For Bayesian analysis, information on the choice of priors and Markov chain Monte Carlo settings |
| <input checked="" type="checkbox"/> | <input type="checkbox"/> For hierarchical and complex designs, identification of the appropriate level for tests and full reporting of outcomes |
| <input checked="" type="checkbox"/> | <input type="checkbox"/> Estimates of effect sizes (e.g. Cohen's d , Pearson's r), indicating how they were calculated |

Our web collection on [statistics for biologists](#) contains articles on many of the points above.

Software and code

Policy information about [availability of computer code](#)

Data collection

Pseudovirus neutralization and ELISA data were collected by microplate spectrophotometer (PerkinElmer, HH3400).
Biolayer interferometry data were collected with Octet Acquisition 9.0 (Fortebio).
FACS data was collected by Summit 6.0 (Beckman Coulter).
SPR data were obtained with BIAcore 8K Evaluation Software (v3.0.12.15655)
Cryo-EM data collection was performed using either a Titan Krios G3 equipped with a K3 direct detection camera, or a Titan Krios G2 with a K2 camera.

Data analysis

Neutralization assays data were analyzed using PRISM (versions 9.0.1) as described in Methods. BLI data analyses were done by Octet Analysis 9.0 (Fortebio) and Octet Analysis Studio 12.2 (Fortebio). SPR data were fitted with Biacore 8K Evaluation Software (v3.0.12.15655). FACS data were analyzed by FlowJo 10.8. V(D)J sequence data were analyzed using Cell Ranger (v6.1.1) and IMG2/DomainGapAlign (v4.10.2), and R packages Seurat (v4.0.3), SingleR (v1.6.1). Illumina barcodes sequencing data from deep mutational scanning experiments were analyzed using custom scripts (<https://github.com/jianfcpku/SARS-CoV-2-RBD-DMS-broad>) and Python package dms_variants (v0.8.9). Logo plots were generated by Python package logomaker (version 0.8) and R package ggseqlogo (version 0.1). For unsupervised clustering, we utilized Python package scikit-learn (version 0.24.2) to perform multidimensional scaling (MDS), k-means clustering and t-Distributed Stochastic Neighbor Embedding (t-SNE) embedding. 2D t-SNE plots are generated by ggplot2 (version 3.3.3). Multiple sequence alignments of sarbecovirus RBD were generated using ClustalOmega (version 1.2.4). Cryo-EM data processing was carried out using cryoSPARC (v3.2.1), UCSF Chimera (v1.16) and Relion (v3.1). MD-simulation based on cryo-EM structures was carried out using GROMACS-2021. Coot (v0.8.9.2) and Phenix (v1.20) were used for cryo-EM structural modeling and refinement. Structure figures were prepared using UCSF ChimeraX (v1.3) and Pymol (v2.6.0a0).

For manuscripts utilizing custom algorithms or software that are central to the research but not yet described in published literature, software must be made available to editors and reviewers. We strongly encourage code deposition in a community repository (e.g. GitHub). See the Nature Portfolio [guidelines for submitting code & software](#) for further information.

Data

Policy information about [availability of data](#)

All manuscripts must include a [data availability statement](#). This statement should provide the following information, where applicable:

- Accession codes, unique identifiers, or web links for publicly available datasets
- A description of any restrictions on data availability
- For clinical datasets or third party data, please ensure that the statement adheres to our [policy](#)

Processed mutation escape scores can be downloaded at <https://github.com/jianfcpku/SARS-CoV-2-RBD-DMS-broad>. Raw Illumina and PacBio sequencing data are available on NCBI Sequence Read Archive BioProject PRJNA804413. We used vdj_GRCh38_alts_ensembl-5.0.0 as the reference of V(D)J alignment, which can be obtained from <https://support.10xgenomics.com/single-cell-vdj/software/downloads/latest>. IMG2/DomainGapAlign is based on the built-in latest IMG2 antibody database, and we let the "Species" parameter as "Homo sapiens" while kept the others as default. Public deep mutational scanning datasets involved in the study from literature could be downloaded at https://media.githubusercontent.com/media/jbloomlab/SARS2_RBD_Ab_escape_maps/main/processed_data/escape_data.csv. Public structures involved in this manuscript were downloaded from Protein Data Bank with accession codes 6M0J, 7K8V, 7MMO, 7EY0, 7DX4, 7M7W, 7JW0, 7WPB, 7WGB.

Cryo-EM density maps have been deposited in the Electron Microscopy Data Bank with accession codes EMD-33210, EMD-33211, EMD-33212, EMD-33213, EMD-33323, EMD-33324, EMD-33325, EMD-32732, EMD-32738, EMD-32734, EMD-32718, and EMD-33019, respectively. Structural coordinates have been deposited in the Protein Data Bank with accession codes 7XIW, 7XIX, 7XIY, 7XIZ, 7XNQ, 7XNR, 7XNS, 7WRL, 7WRZ, 7WRO, 7WR8 and 7X6A.

Field-specific reporting

Please select the one below that is the best fit for your research. If you are not sure, read the appropriate sections before making your selection.

- Life sciences Behavioural & social sciences Ecological, evolutionary & environmental sciences

For a reference copy of the document with all sections, see [nature.com/documents/nr-reporting-summary-flat.pdf](https://www.nature.com/documents/nr-reporting-summary-flat.pdf)

Life sciences study design

All studies must disclose on these points even when the disclosure is negative.

Sample size	A total of 1640 antibodies were characterized in the manuscript. No sample size calculation was performed. The sample size of this study was chosen to obtain sufficient antibodies in each epitope group. Plasma samples were obtained from 40 volunteers who received 3 doses of CoronaVac, 38 individuals who received 2 doses of CoronaVac and 1 booster dose of ZF2001, 50 BA.1 convalescents who had received 3 doses of CoronaVac before BA.1 infection, and 28 SARS convalescents who received 2 doses of CoronaVac and 1 dose of ZF2001. No sample size calculation was performed. All samples obtained were analyzed.
Data exclusions	457 antibodies were excluded from the study because of insufficient antibody or meaningless deep mutation screening results, which defined as no mutations scored two times of the median score.
Replication	Experimental assays were performed in biological duplicate according to or exceeding standards in the field. Specifically, we perform MACS-based mutation screening using two independently synthesized mutant libraries. We conducted all neutralization and ELISA assays in biological replicates. SPR and BLI measurements are all performed in at least two biological replicates. All replicates for neutralization, ELISA, SPR and BLI assays are successful.
Randomization	Randomization was not required since we were applying a uniform set of measurements across the panel of monoclonal antibodies and plasma. As this is an observational study, randomization is not relevant.
Blinding	Blinding was not required since we were applying a uniform set of measurements across the panel of monoclonal antibodies and plasma. As this is an observational study, investigators were not blinded.

Reporting for specific materials, systems and methods

We require information from authors about some types of materials, experimental systems and methods used in many studies. Here, indicate whether each material, system or method listed is relevant to your study. If you are not sure if a list item applies to your research, read the appropriate section before selecting a response.

Materials & experimental systems

n/a	Included in the study
<input type="checkbox"/>	<input checked="" type="checkbox"/> Antibodies
<input type="checkbox"/>	<input checked="" type="checkbox"/> Eukaryotic cell lines
<input checked="" type="checkbox"/>	<input type="checkbox"/> Palaeontology and archaeology
<input checked="" type="checkbox"/>	<input type="checkbox"/> Animals and other organisms
<input type="checkbox"/>	<input checked="" type="checkbox"/> Human research participants
<input checked="" type="checkbox"/>	<input type="checkbox"/> Clinical data
<input checked="" type="checkbox"/>	<input type="checkbox"/> Dual use research of concern

Methods

n/a	Included in the study
<input checked="" type="checkbox"/>	<input type="checkbox"/> ChIP-seq
<input type="checkbox"/>	<input checked="" type="checkbox"/> Flow cytometry
<input checked="" type="checkbox"/>	<input type="checkbox"/> MRI-based neuroimaging

Antibodies

Antibodies used

ELISA: goat anti-human IgG(H+L)HRP (JACKSON, 109-035-003)
 The enriched B cells were stained with FITC anti-human CD19 antibody (BioLegend, 392508), FITC anti-human CD20 antibody (BioLegend, 302304), Brilliant Violet 421 anti-human CD27 antibody (BioLegend, 302824), PE/Cyanine7 anti-human IgM antibody (BioLegend, 314532), PE/Cyanine7 anti-human IgD antibody (BioLegend, 348210), biotinylated SARS-CoV-2 BA.1 protein (His & AVI Tag) (SinoBiological, 40592-V49H7-B) conjugated with PE-streptavidin (BioLegend, 405204), APC-streptavidin (BioLegend, 405207), TotalSeq™-C0971 Streptavidin (BioLegend, 405271), and TotalSeq™-C0972 Streptavidin (BioLegend, 405273), SARS-CoV-2 biotinylated RBD protein (His & AVI Tag) conjugated with Brilliant Violet 605™ Streptavidin, TotalSeq™-C0973 Streptavidin (BioLegend, 405275), TotalSeq™-C0974 Streptavidin (BioLegend, 405277), biotinylated Ovalbumin conjugated with TotalSeq™-C0975 Streptavidin (BioLegend, 405279) and 7-AAD (Invitrogen, 00-6993-50).
 All human antibodies were expressed using HEK293F cell lines with codon-optimized cDNA and human IgG1 constant regions in house. The detailed sequence could be found in Supplementary material.

Validation

In this manuscript, we tested 1640 human IgG1 antibodies. All antibodies were expressed using HEK293F cell lines with codon-optimized cDNA and human IgG1 constant regions. All antibodies' species and specificity to RBD were validated by ELISA. All antibodies neutralization ability was verified by VSV-based pseudotyped virus assays. Details and sequences for all SARS-CoV-2 antibodies evaluated in this study is included in Supplementary Table 2.
 Reactivity and specificity of the primary antibodies listed above is based on the information on manufacturer's websites:
 Goat anti-human IgG(H+L)HRP (JACKSON, 109-035-003): Based on immunoelectrophoresis and/or ELISA, the antibody reacts with whole molecule human IgG. It also reacts with the light chains of other human immunoglobulins. No antibody was detected against non-immunoglobulin serum proteins. The antibody may cross-react with immunoglobulins from other species.
 FITC anti-human CD19 antibody was validated by successful staining and FC analysis according to the manufacturer's website <https://www.biolegend.com/en-us/products/fitc-anti-human-cd19-antibody-16221> and previous publication: Riquelme SA, et al. 2020. Cell Metabolism. 31(6):1091-1106.e6.
 FITC anti-human CD20 antibody was validated by successful staining and FC analysis according to the manufacturer's website <https://www.biolegend.com/en-us/products/fitc-anti-human-cd20-antibody-558> and previous publication: Mishra A, et al. 2021. Cell. 184(13):3394-3409.e20.
 Brilliant Violet 421 anti-human CD27 antibody was validated by successful staining and FC analysis according to the manufacturer's website <https://www.biolegend.com/en-us/products/brilliant-violet-421-anti-human-cd27-antibody-7276> and previous publication: Dugan HL, et al. 2021. Immunity. 54(6):1290-1303.e7.
 PE/Cyanine7 anti-human IgM antibody was validated by successful staining and FC analysis according to the manufacturer's website <https://www.biolegend.com/en-us/products/pe-cyanine7-anti-human-igm-antibody-12467> and previous publication: Shehata L, et al. 2019. Nat Commun. 10:1126.
 PE/Cyanine7 anti-human IgD antibody was validated by successful staining and FC analysis according to the manufacturer's website <https://www.biolegend.com/en-us/products/pe-cyanine7-anti-human-igd-antibody-6996> and previous publication: Ahmed R et al. 2019. Cell. 177(6):1583-1599.

Eukaryotic cell lines

Policy information about cell lines

Cell line source(s)

HEK293F for antibody and sarbecovirus RBD production was received from ThermoFisher (R79007);
 EBV100 (Yeast) was received from ATCC (ATCCMYA-4941);
 Huh-7 for pseudovirus assays was received from Japanese Collection of Research Bioresources (JCRB 0403) ;
 293T-hACE2 cells for pseudovirus assays was received from ATCC (CRL-3216) ;

Authentication

No authentication was performed beyond manufacturer standards;

Mycoplasma contamination

Not tested for mycoplasma contamination;

Commonly misidentified lines
(See [ICLAC](#) register)

No commonly misidentified cell lines were used in the study.

Human research participants

Policy information about [studies involving human research participants](#)

Population characteristics

Plasma samples were obtained from 40 volunteers who received 3 doses of CoronaVac, 38 individuals who received 2 doses of CoronaVac and 1 booster dose of ZF2001, 50 BA.1 convalescents who had received 3 doses of CoronaVac before BA.1 infection, and 28 SARS convalescents who received 2 doses of CoronaVac and 1 dose of ZF2001. For the CoronaVac-boosted cohort, individuals were vaccinated by 2 doses of CoronaVac and boosted with CoronaVac six months after the second dose. The blood samples were obtained 4 weeks after the booster dose (21-59 years old, 9/40 male, 31/40 female). For the ZF2001-boosted cohort, individuals were vaccinated by 2 doses of CoronaVac and boosted with ZF2001 six months after the second dose. The blood samples were obtained 4 weeks after the booster dose (20-57 years old, 11/38 male, 27/38 female). For the BA.1 breakthrough infection cohort, the blood samples were obtained 4 weeks after hospitalization discharge (23-63 years old, 28/50 male, 22/50 female, 24/50 diagnosed as mild COVID-19, 26/50 diagnosed as moderate COVID-19, all received 2 doses of CoronaVac and a CoronaVac booster dose six months after the second dose before infection). We presume all individuals were infected by BA.1 since these individuals were infected during the BA.1 wave in Tianjin, China in Jan 2022. A total of 430 patients were confirmed infected and no other lineages were detected beside BA.1 by sequencing in that wave. For the SARS convalescents, all individuals were infected by SARS-CoV-1 in 2003 in Beijing, China and vaccinated by 2 doses of CoronaVac and boosted with ZF2001 six months after the second dose. The blood samples were collected 4 weeks after the booster dose (39-76 years old, 10/28 male, 18/28 female). Detailed population characteristics and vaccination profiles are described in Supplementary Table 1.

Recruitment

Patients were recruited on the basis of SARS-CoV-1 infection, BA.1 infection and SARS-CoV-2 vaccination. The only exclusion criteria used were HIV or other debilitating diseases. All SARS convalescents were infected by SARS-CoV-1 in 2003; thus, the average age of this cohort is older than other cohorts involved in this study. This may cause a systematically lower humoral immunity response in the SARS convalescents cohort.

Ethics oversight

This study was approved by the Ethics Committee of Beijing Ditan Hospital affiliated to Capital Medical University (Ethics committee archiving No. LL-2021-024-02), the Tianjin Municipal Health Commission, and the Ethics Committee of Tianjin First Central Hospital (Ethics committee archiving No. 2022N045KY). Written informed consent was obtained from each participant in accordance with the Declaration of Helsinki. All participants provided written informed consent for the collection of information, and that their clinical samples were stored and used for research. Data generated from the research were agreed to be published.

Note that full information on the approval of the study protocol must also be provided in the manuscript.

Flow Cytometry

Plots

Confirm that:

- The axis labels state the marker and fluorochrome used (e.g. CD4-FITC).
- The axis scales are clearly visible. Include numbers along axes only for bottom left plot of group (a 'group' is an analysis of identical markers).
- All plots are contour plots with outliers or pseudocolor plots.
- A numerical value for number of cells or percentage (with statistics) is provided.

Methodology

Sample preparation

Whole blood samples from SARS-CoV-2, SARS convalescents or vaccinees were mixed and subjected to Ficoll (Cytiva, 17-1440-03) gradient centrifugation after 1:1 dilution in PBS+2% FBS. After centrifugation, plasma was collected from upper layer and cells were harvested at the interface, respectively. PBMCs were further prepared through centrifugation, red blood cells lysis (Invitrogen™ eBioscience™ 1X RBC Lysis Buffer, 00-4333-57) and washing steps. Samples were stored in FBS (Gibco) with 10% DMSO (Sigma) in liquid nitrogen if not used for downstream process immediately. Cryopreserved PBMCs were thawed in DPBS+2% FBS (Stemcell, 07905). On the day of sorting, B cells were enriched using CD19+ B cell isolation kit according to the manufacturer's instructions (STEMCELL, 19054). Enriched B cells were then stained with FITC anti-human CD20 antibody, Brilliant Violet 421™ anti-human CD27 antibody, PE/Cyanine7 anti-human IgM antibody, PE/Cyanine7 anti-human IgD antibody (BioLegend, 348210), biotinylated SARS-CoV-2 BA.1 protein (His & AVI Tag) (SinoBiological, 40592-V49H7-B) conjugated with PE-streptavidin, APC-streptavidin, TotalSeq™-C0971 Streptavidin (BioLegend, 405271), and TotalSeq™-C0972 Streptavidin (BioLegend, 405273), SARS-CoV-2 biotinylated RBD protein (His & AVI Tag) conjugated with Brilliant Violet 605™ Streptavidin, TotalSeq™-C0973 Streptavidin (BioLegend, 405275), TotalSeq™-C0974 Streptavidin (BioLegend, 405277), biotinylated Ovalbumin conjugated with TotalSeq™-C0975 Streptavidin (BioLegend, 405279) and 7-AAD.

Instrument

Astrios EQ (BeckMan Coulter)

Software	Summit 6.0 (Beckman Coulter) for cell sorting; FlowJo 10.8 for data analysis.
Cell population abundance	Memory B cell purity post-sorting is over 90% as measured by 10x sequencing.
Gating strategy	7-AAD-, CD20+, CD27+, IgM-, IgD-, SARS-CoV-2 BA.1 RBD+ B cells were sorted on an Astrios EQ (BeckMan Coulter) into PBS containing 30% FBS. The detailed FSC/SSC gating scheme is showed in Extended Data Figure 2. Gates are drawn to define positive cells on the basis of unvaccinated healthy donor control.

Tick this box to confirm that a figure exemplifying the gating strategy is provided in the Supplementary Information.